LIMNOLOGY and OCEANOGRAPHY

ASLO

Limnol. Oceanogr. 68, 2023, 2544–2561

doi: 10.1002/lno.12440

Uptake of barium, molybdenum, and lithium and incorporation into scallop shells: Refining proxies for primary production dynamics

Lukas Fröhlich,[1*] **Valentin Siebert**,[2] **Qian Huang**,[1] **Julien Thébault**,[2] **Brivaëla Moriceau**,[2] **Klaus Peter Jochum**,[3] **Bernd R. Schöne**[1]

[1]Institute of Geosciences, University of Mainz, Mainz, Germany
[2]Univ Brest, CNRS, IRD, Plouzané, France
[3]Climate Geochemistry Department, Max Planck Institute for Chemistry, Mainz, Germany

Abstract

Ba/Ca_{shell}, Mo/Ca_{shell}, and Li/Ca_{shell} chronologies of *Pecten maximus* can provide information on past phytoplankton dynamics. Distinct Ba, Mo, and Li peaks in the shells are associated with algal blooms. This study evaluated the underlying hypothesis that respective element profiles reliably record variations in phytoplankton dynamics occurring within the water column. Therefore, the chemical content of scallops from the Bay of Brest, France, that lived on the sediment surface was compared to conspecific specimens living in a cage above the seafloor and compared with the phytoplankton abundance and the physicochemical properties of the water column. As demonstrated, Ba/Ca_{shell} and Mo/Ca_{shell} peaks occurred contemporaneously in specimens within the cage and on the sediment, but were higher in the latter. Furthermore, element/Ca peaks agreed with the timing of particulate Ba and Mo enrichments in the seawater. These data support the assumption of a dietary uptake of both elements. Differences in peak heights between shells living in a cage and on the seafloor were controlled by rates of filtration and biomineralization. While the timing and magnitude of Ba/Ca_{shell} peaks were linked to Ba-containing diatoms, Mo/Ca_{shell} peaks were related to blooms of Mo-enriched dinoflagellate and diatom aggregation events. Two episodes of slight Li enrichment occurred synchronously in cage and sediment shells. Although the exact mechanism causing such Li increases remains unresolved, the findings suggest a link to large diatom blooms or the presence of a specific diatom taxon. This study refines previously hypothesized relationships between trace element enrichments in scallop shells and phytoplankton dynamics.

The health of aquatic ecosystems is strongly influenced by phytoplankton. Besides producing oxygen and sequestering atmospheric CO_2 (Field et al. 1998; Westberry et al. 2008), phytoplankton also impacts marine food webs (e.g., Turner and Tester 1997). Increasing surface water temperature (Winder and Sommer 2012), ocean acidification (Iglesias-Rodriguez et al. 2008) and imbalanced levels of nutrients caused by inputs of anthropogenic pollutants and artificial fertilizers (Vitousek et al. 1997) can affect the phytoplankton species abundance and community structure. Nearshore areas that provide the habitat for many organisms and serve as valuable sites for human activities (e.g., Worm et al. 2006; Barbier et al. 2011) are particularly vulnerable to eutrophication-induced changes in the phytoplankton species composition. For example, the transition from a phytoplankton community dominated by diatoms to such largely dominated by non-siliceous species such as dinoflagellates (e.g., Wasmund et al. 2017; Spilling et al. 2018) can lead to an increase in harmful algal blooms (Hallegraeff 1993; Lewitus et al. 2012). To evaluate future trends in phytoplankton community structures, it is crucial to understand the preindustrial phytoplankton dynamics. Such an approach requires temporally well-constrained archives, for example, shells of bivalve mollusks, which reliably record ephemeral variations in phytoplankton species dynamics.

Bivalves record paleoenvironmental information in their shells at high temporal resolution, specifically in the form of geochemical properties, including stable isotopes (e.g., Schöne

*Correspondence: lufroehl@uni-mainz.de

Additional Supporting Information may be found in the online version of this article.

Author Contribution Statement: L.F., Q.H. and B.R.S. conceptualized the study. V.S., J.T., B.M. and L.F. performed investigation and data curation. B.R.S., J.T. and K.P.J. provided the resources. L.F. wrote the original draft and did the visualization. V.S., Q.H., J.T., B.M., K.P.J. and B.R.S. were involved in reviewing and editing of the manuscript. B.R.S. and J.T. managed the supervision as well as the project administration and acquired funding for this study. All authors contributed substantially to the drafts and provided final approval for publication.

et al. 2003; McConnaughey and Gillikin 2008) as well as trace and minor elements (e.g., Thébault et al. 2009*b*; Zhao et al. 2017; Schöne et al. 2021). Daily, fortnightly and annual growth increments and lines (e.g., Chauvaud et al. 1998; Clark 2005) can be used to temporally contextualize these geochemical properties. Temporally constrained barium-to-calcium ratios in shells (Ba/Ca_{shell}) of different bivalve species, for example, *Arctica islandica*, *Glycymeris pilosa*, and *Pecten maximus*, were identified as proxies for phytoplankton dynamics (e.g., Stecher et al. 1996; Gillikin et al. 2006). Respective time series were characterized by a low background that was interrupted by sharp, erratic peaks. Notably, Ba/Ca_{shell} peaks occurred highly synchronously among specimens growing at the same locality and time (e.g., Gillikin et al. 2008; Barats et al. 2009; Thébault et al. 2009*a*). Whereas Ba/Ca_{shell} peaks typically correlate weakly with chlorophyll *a* concentration (e.g., Gillikin et al. 2008; Fröhlich et al. 2022*b*; Schöne et al. 2023), they seem to be strongly linked to blooms of specific phytoplankton taxa, especially diatoms containing species-specific loads of cellular Ba (e.g., Roth and Riley 1971; Fisher et al. 1991; Sternberg et al. 2005). Furthermore, profiles of molybdenum-to-calcium ratios (Mo/Ca) and lithium-to-calcium ratios (Li/Ca) in scallop shells exhibited similar patterns as Ba/Ca_{shell}. These patterns include a low background level interrupted by sharp peaks and were likewise associated with phytoplankton dynamics (Thébault et al. 2009*a*, 2022; Barats et al. 2010; Thébault and Chauvaud 2013). However, the underlying mechanisms leading to the formation of Mo/Ca_{shell} and Li/Ca_{shell} peaks differed notably from those of Ba/Ca_{shell} peaks. Enhanced dietary uptake of Mo by *P. maximus* (Barats et al. 2010; Tabouret et al. 2012) seems to be related to the ingestion of small Mo-enriched aggregates of phytoplankton cells (Thébault et al. 2022) and specific dinoflagellates with a high load of cellular Mo (Fröhlich et al. 2022*a*). Yet, it remains unresolved if these mechanisms provide sufficient quantities of Mo that can explain the formation and magnitude of Mo/Ca_{shell} peaks. The timing of Li/Ca_{shell} peaks in shells of *P. maximus* suggested a relationship to blooms of diatoms adsorbing Li from the water column (Thébault and Chauvaud 2013; Thébault et al. 2022). Thus, Ba/Ca_{shell}, Mo/Ca_{shell}, and Li/Ca_{shell} profiles of scallops seem to serve as highly valuable sclerochronological tools to derive information about past phytoplankton dynamics. However, despite an increasing number of implications for a trophic uptake of Ba, Mo, and Li, uncertainties remain to what extent the complex dynamics of phytoplankton contribute to the shell geochemistry and which pathways (uptake of these elements, transport within the body and incorporation into the shell) are involved. For instance, the large variation of cellular Ba reported in various marine phytoplankton taxa (e.g., Fisher et al. 1991; Masuzawa et al. 1999; Lobus et al. 2021) makes it difficult to precisely attribute Ba/Ca_{shell} peaks to the presence of specific phytoplankton taxa. To use Ba/Ca_{shell}, Mo/Ca_{shell}, and Li/Ca_{shell} as qualitative and quantitative proxies for phytoplankton dynamics, more detailed information is required on the elemental uptake and shell incorporation, which control the formation of peaks in the trace element-to-calcium profiles.

This study combines highly resolved time series of Ba/Ca_{shell}, Mo/Ca_{shell}, and Li/Ca_{shell} measured in contemporaneous *P. maximus* specimens (Bay of Brest, France) with detailed environmental monitoring data (Siebert et al. 2023), aiming to verify and refine proposed hypotheses about the uptake of Ba, Mo, and Li from the ambient environment into the shells. Specifically, it was tested that phytoplankton-related processes occurring within the water column affect the chemical composition of scallop shells, substantiating these shells as reliable geochemical archives to accurately record respective events. This was achieved by comparing element chemical properties of scallops that thrived naturally on the sediment surface to such specimens that lived inside a cage deployed above the seafloor. Geochemical data from the two settings (sediment floor and cage) were also compared with the chemistry of the ambient seawater and the prevailing phytoplankton dynamics. Together with specimen-specific physiological parameters, the molar element-to-calcium ratios were used to deduce absolute concentrations of trace elements that were potentially taken up by the scallops. This novel approach allowed us to quantitatively evaluate if the proposed uptake mechanisms provide sufficient quantities of trace elements to explain their enrichment in the shells. The results of this study can increase the understanding of how Ba/Ca_{shell}, Mo/Ca_{shell}, and Li/Ca_{shell} of *P. maximus* respond to variations in the ambient environment and facilitate the use of the shells as archives for past phytoplankton dynamics.

Material and methods

Study locality, shell collection, and experimental setup

In October 2021, living specimens of *P. maximus* were collected by SCUBA divers in the southern part of the Bay of Brest (Pointe de Lanvéoc, 48°17′39″N, 004°27′12″W [WGS84]; Supporting Information Fig. S1). The bay is a typical shallow (8–15 m depth) and semi-enclosed coastal ecosystem in northwestern France that has been extensively researched in ecological and phytoplankton-related studies over the past years. This constitutes the Bay of Brest as an ideal location to study potential geochemical responses in scallop shells to environmental signals such as large phytoplankton blooms whose initiation is largely controlled by sea surface temperature, nutrient inputs, light conditions, and ocean currents (e.g., Poppeschi et al. 2022). Six specimens were collected from their natural habitat, specifically, scallops that lived and grew on the sediment surface (at approximately 8 m below sea surface; hereafter, these shells are referred to as "sediment shells"), and six specimens were retrieved from cages (hereafter referred to as "cage shells") positioned about 1 m above the sediment–water interface (i.e., thin layer at the boundary between sediment surface and water column; SWI) (*see* Supporting Information Table S1). These large-meshed cages (approximately 0.5 cm

mesh size, 60 cm × 80 cm × 25 cm) were deployed on 22 February 2021 and juvenile scallops (obtained from the Tinduff Hatchery in Plougastel-Daoulas, France, with a shell height between 2.5 and 3 cm) placed inside (30 scallops per cage). All specimens used in this study have encountered one winter (age class 1) showing a prominent winter growth line (Supporting Information Fig. S1). *P. maximus* precipitates most of the shell carbonate during the second year of life. The respective shell portion, therefore, provides the highest temporal resolution for sclerochronological analyses. After collection, the bivalves were dissected, eviscerated, and epibionts gently removed with a nylon brush. For shell growth pattern and element chemical analyses (for a detailed description of LA-ICP-MS and growth pattern analyses as well as temporal contextualization of geochemical data, *see* Supporting Information), only the left (flat) valves were utilized because these valves show the most distinct daily growth patterns (growth increments and growth lines, aka "striae"; Chauvaud et al. 1998). In all cage specimens, shell portions representing the beginning of the growing period in March/April were infested by epibionts, leading to difficulties in the identification of individual growth increments and in situ element analyses. Accordingly, only shell portions without epibionts were used in this study. Water samples collected at the same locality as the scallop specimens were analyzed for their phytoplankton compositions, element chemical properties in the particulate fraction (PBa, PMo, and PLi) as well as for their particulate organic carbon (POC) content (details provided in the Supporting Information).

Trace element uptake by scallops and relation to phytoplankton

Based on the molar trace element-to-calcium ratios measured in the scallop shells, the absolute amount of trace elements incorporated into the shell per day was calculated following the method described by Thébault et al. (2009*a*). In addition, the quantity of a trace element contained in each liter of filtered seawater was deduced from the Ba/Ca_{shell}, Mo/Ca_{shell}, and Li/Ca_{shell} profiles. Briefly, the calculations were based on the following model, with daily growth rates and molar element-to-calcium ratios as input parameters (model described and illustrated in the Supporting Information and Supporting Information Fig. S2A): (1) The shell growth rates were used to calculate the total shell height at each day. (2) The soft tissue dry weight was estimated using the previously determined relationship between shell height and soft tissue dry weight that was previously described for *P. maximus* (Lorrain et al. 2004). (3) Similarly, the shell height was used to account for the shell weight using the shell height-to-shell weight relationship of *P. maximus* (Lorrain et al. 2004). (4) Daily filtration rates were deduced from the soft tissue weight and a soft tissue dry weight-standardized filtration rate of $\sim 5\ L\ h^{-1}\ g^{-1}$ (Palmer 1980; Laing 2004; Thébault et al. 2009*a*). (5) The shell weight was used to estimate the amount of shell material that was precipitated each day. (6) The absolute amount of a trace element that was incorporated into the shell during each day was estimated according to the measured trace element-to-calcium ratios and a relative Ca content of 38 wt% (determined for *P. maximus* by Richard 2009 and *A. islandica* shells by Marali et al. 2017) of the total shell material. Background subtraction was performed for the Ba/Ca_{shell} and Mo/Ca_{shell} profiles to remove the influence of dissolved Ba and Mo on the measured element-to-calcium ratios, using the partition coefficient for Ba ($D_{Ba} = 0.11$; Barats et al. 2009) and Mo ($D_{Mo} = 1.5 \times 10^{-4}$; Barats et al. 2010). The relationship between daily growth rates and Li/Ca_{shell} background was used to account for excess Li/Ca_{shell} (Thébault and Chauvaud 2013). (7) The amount of trace elements that was contained in each liter of filtered seawater (hereafter referred to as $TE_{filtered\ seawater}$) was estimated considering the total load of trace elements incorporated into the bivalve (assuming that 63% of the total Ba and 27% of the total Mo ends up in the shell matrix according to preliminary data from Barats 2006) each day and the daily filtration rate. Absolute estimates of $Li_{filtered\ seawater}$ were not obtained as the relative distribution of Li among the soft tissue and shell material was not available.

To quantify the potential trace element content in phytoplankton, the estimated $TE_{filtered\ seawater}$ levels were compared with the measured phytoplankton cell concentration data based on previously hypothesized relationships between trace element incorporation rates and phytoplankton dynamics. The uptake mechanisms were quantitatively evaluated for Ba and Mo, but only qualitatively for Li because absolute values for $Li_{filtered\ seawater}$ could not be obtained (*see* above). Accordingly, $Mo_{filtered\ seawater}$ levels were related to the cell concentration data of the dinoflagellate genus *Gymnodinium* spp. (Fröhlich et al. 2022*a*). In contrast to Mo/Ca_{shell}, the patterns of the Ba/Ca_{shell} profiles were hypothesized to be controlled by the abundance of multiple phytoplankton species, primarily diatoms (Thébault et al. 2009*a*; Fröhlich et al. 2022*a*,*b*). To detect potential patterns between the Ba/Ca_{shell} profiles and diatoms, the pseudo-random Monte Carlo (MC) approach described in Fröhlich et al. (2022*a*) was used. Given the premise that Ba/Ca_{shell} peaks follow the timing and intensity of phytoplankton blooms, along with species-specific amounts of cell-associated Ba, this method evaluated numerous potential scenarios (i.e., 1.8×10^9) and identified the statistically most relevant one. To this avail, combinations of phytoplankton cell concentration data (determined for specific phytoplankton taxa) were pseudo-randomly selected, temporally shifted (within a predefined time window, i.e., time lag), weighted (between 0 and 1), and merged into artificially generated time series (for details *see* Fröhlich et al. 2022*a*). Then, the resulting time series were correlated with the Ba/Ca_{shell} profile using the Pearson correlation coefficient as a metric. Note that uncertainties in the temporal alignment of the geochemical shell data, as well as the low sampling frequency of the phytoplankton data (i.e., the exact timing when a

phytoplankton bloom reaches the highest cell concentration remains unknown), largely influence the direct assignment of a given phytoplankton bloom to a Ba/Ca_{shell} peak during the MC calculations. In addition, a short time lag of up to 12 d between the occurrence of a given phytoplankton species and a Ba/Ca_{shell} peak had to be assumed (Fröhlich et al. 2022*a*,*b*). Therefore, stepwise testing of different time windows (i.e., 4-d window) was necessary to determine the combination of different phytoplankton species that agreed best with the measured Ba/Ca_{shell} profile. As no phytoplankton data were available for the time between late July and early September, the MC approximations were performed, excluding this time interval. The MC-estimated species-specific weighting coefficients served as relative Ba-enrichment factors and were used together with $Ba_{filtered\ seawater}$ to account for the minimum content of diatom-associated Ba in 1 L of seawater that was potentially ingested by the scallops (*see* Fig. S2B).

Results

Ba in shells, seawater, and relation to diatom blooms

All studied cage shells (Fig. 1A; Supporting Information Fig. S4A) showed one prominent Ba/Ca_{shell} peak at ca. 08 June that occurred simultaneously in all specimens from the cage (on average, $5.23 \pm 0.79\ \mu mol\ mol^{-1}$). This peak was followed by another, smaller Ba/Ca_{shell} enrichment (04 July; on average $2.37\ \mu mol\ mol^{-1}$), which was, however, only well-pronounced in one of the three studied specimens (Shell B; Supporting Information Fig. S4A). Similarly, in late July, another Ba/Ca_{shell} peak was only observed in one of the three specimens (Shell C; Supporting Information Fig. S4A). On average, the measured Ba/Ca_{shell} background in cage shells was around $1.73 \pm 0.41\ \mu mol\ mol^{-1}$. In the ontogenetically older shell portions (starting from mid-August), larger deviations from this background level were observed as short-term (< 2 d) enrichments showing Ba/Ca_{shell} ratios reaching up to $8.23\ \mu mol\ mol^{-1}$ on 05 September in Shell A (Fig. 1A).

In contrast to the cage shells, the Ba/Ca_{shell} profiles of sediment specimens revealed a more stable background level of about $0.96 \pm 0.20\ \mu mol\ mol^{-1}$ (Fig. 1A). This background was interrupted by a large double peak between late May and end of June, with average values of 9.50 and $4.80\ \mu mol\ mol^{-1}$ on 08 June and 01 July, respectively (Fig. 1A). Although the first Ba/Ca_{shell} peak occurred nearly synchronously in all three specimens (i.e., within a few days), the peak magnitude of Shell D ($18.58\ \mu mol\ mol^{-1}$) was notably larger than that of Shell E and F (5.95 and $7.43\ \mu mol\ mol^{-1}$, respectively; Supporting Information Fig. S4A). In late July, another Ba/Ca_{shell} enrichment episode was observed in all three shells with average values of up to $2.43\ \mu mol\ mol^{-1}$ (25 July). The fourth and last Ba/Ca_{shell} enrichment ($3.86\ \mu mol\ mol^{-1}$) was recorded in August in only one specimen from the sediment (Shell F), while no peak was present in the other two shells (Shells D and E; Supporting Information Fig. S4A). The average background signals differed significantly between cage and sediment shells (approximately 80% higher median in cage shells than in sediment shells), as indicated by a Kruskal–Wallis test ($p < 0.001$, $H[\chi^2] = 135.7$; details about statistics provided in the Supporting Information).

Ratios of PBa to POC (PBa/POC) range from 1.86 to $904.58\ \mu mol\ mol^{-1}$ in bottom waters and 5.23 to $1098.04\ \mu mol\ mol^{-1}$ in surface waters (Fig. 2). PBa/POC profiles at both settings (surface and bottom) were characterized by a very low and flat baseline episodically interrupted by sharp peaks. The largest values were recorded on 07 June in bottom waters and 06 September in surface waters. Notably, all episodes of enhanced PBa/POC ratios that were measured in bottom waters occurred simultaneously with PBa/POC peaks in surface waters, although to different magnitudes. A significant correlation existed between Ba/Ca_{shell} profiles (cage and sediment) and PBa/POC ratios of bottom waters (*see* Supporting Information Fig. S5).

The different Ba/Ca_{shell} enrichments were associated with unique diatom assemblages (Fig. 2). For instance, the two large Ba/Ca_{shell} peaks in shells from the sediment (i.e., in early June and early July; Fig. 2) occurred contemporaneously with blooms of the diatom genus *Leptocylindrus* (i.e., *Leptocylindrus danicus* on 03 June and *L. danicus* + *Leptocylindrus convexus* on

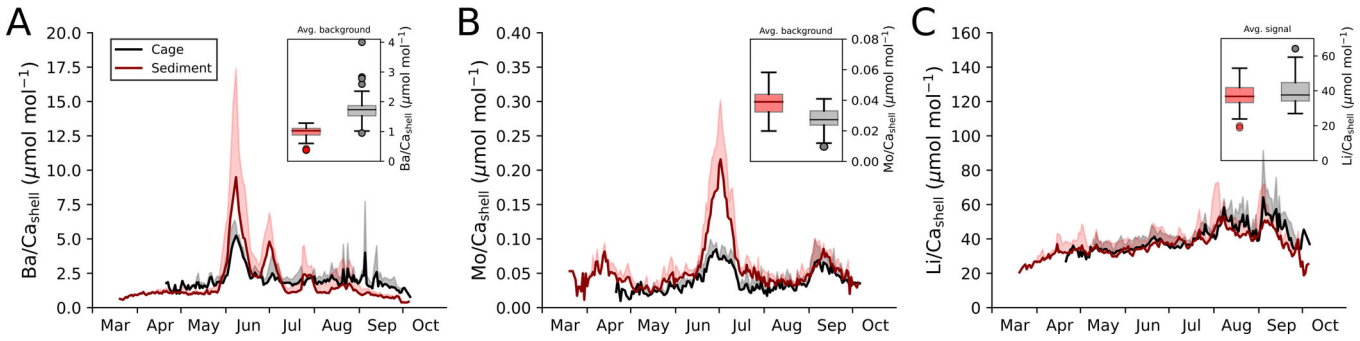

Fig. 1. Averaged Ba/Ca_{shell} (**A**), Mo/Ca_{shell} (**B**), and Li/Ca_{shell} (**C**) profiles ($+1\sigma$) obtained from three *Pecten maximus* specimens grown inside a cage (black) and on the sediment surface (red) during 2021. Box plots indicate differences in the background signals between cage and sediment shells of average Ba/Ca_{shell} and Mo/Ca_{shell} profiles and the average signal of Li/Ca_{shell} ratios.

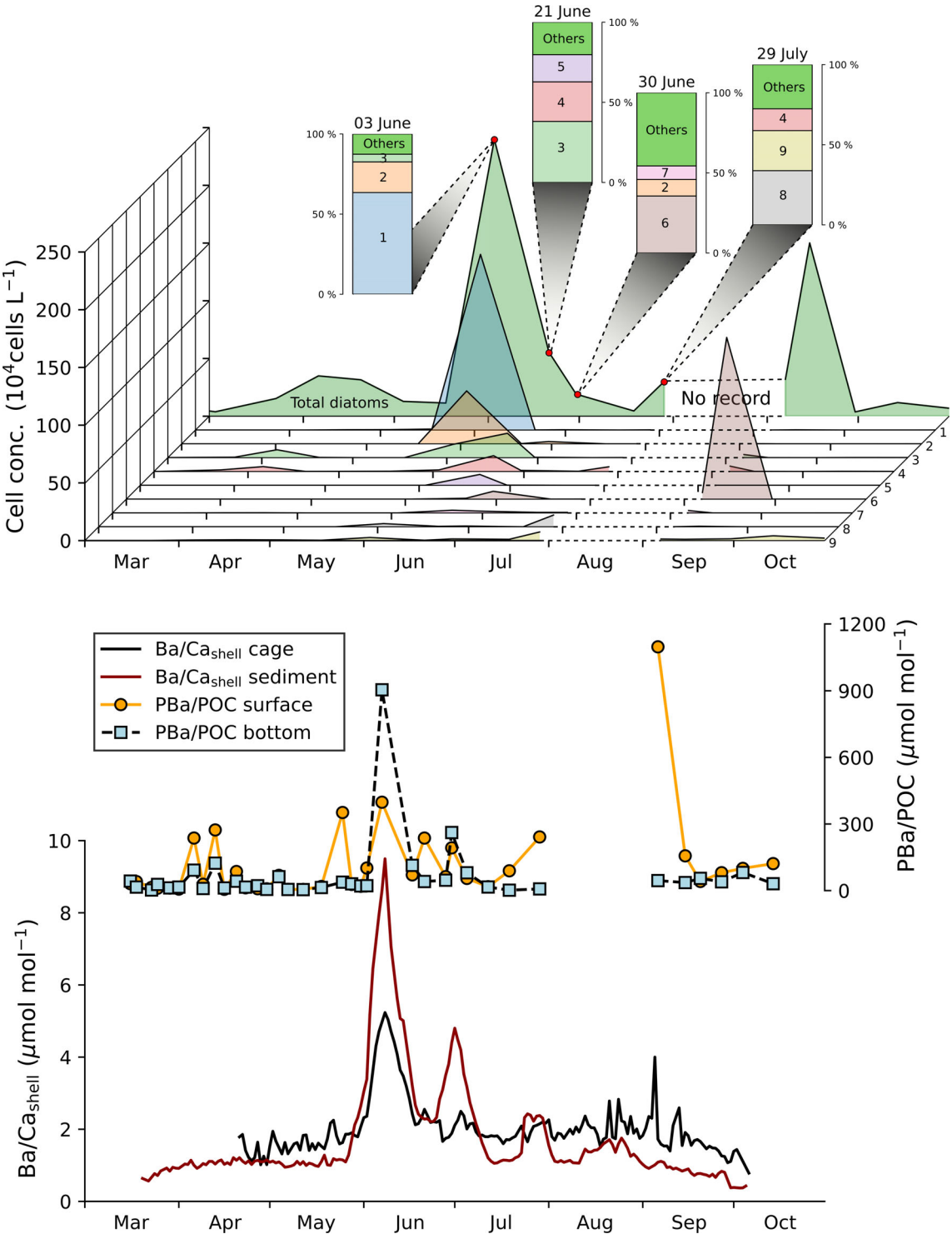

Fig. 2. Average Ba/Ca$_{shell}$ profiles from cage and sediment shells (from 2021), the temporal variation in the PBa/POC ratios measured in surface and bottom waters and the cell concentration time series of the most abundant diatom species that were recorded in the water column (at the studied locality in Lanvéoc, France). The vertical bar plots in the upper panel indicate the relative community compositions at four different dates with the three most abundant diatom taxa (1—*Leptocylindrus danicus*, 2—*Tenuicylindrus belgicus*, 3—*Chaetoceros curvisetus*, 4—*Chaetoceros* spp., 5—*Chaetoceros socialis*, 6—*L. danicus* and *Leptocylindrus convexus*, 7—*C. socialis*, 8—*Pseudo-nitzschia delicatissima*, *Pseudo-nitzschia pseudodelicatissima*, and *Pseudo-nitzschia cuspidata*, 9—*Lennoxia faveolata*).

30 June, respectively), while different diatoms of the genus *Chaetoceros* made up the majority of diatom cells on 21 June that coincided with only a very small Ba/Ca_{shell} enrichment in the cage shells (Fig. 2). No apparent correlation existed between bulk diatom dynamics and Ba/Ca_{shell} profiles. Instead, the pseudo-random MC method revealed potential patterns between Ba/Ca_{shell} profiles and the main abundant diatom taxa (*see* caption Fig. 2). The strongest correlation (Pearson coefficient: 0.91 with $p < 0.05$) between MC-approximated patterns and the Ba/Ca_{shell} profile was obtained for a time lag of 5–8 d (Supporting Information Fig. S6). However, the timing and magnitude of the diatom occurrences agreed better with the Ba/Ca_{shell} profiles at a shorter time lag of 4–7 d (with slightly lower Pearson correlation coefficients). According to this, the best diatom combination (hereafter referred to as "scenario 1," containing the diatom species *Lennoxia faveolata*, *Chaetoceros socialis* and *Chaetoceros laciniosus*, and *Tenuicylindrus belgicus*) coincides with the timing of the two large Ba/Ca_{shell} peaks in June and July and the smaller enrichment at the end of July (Fig. 3; Supporting Information Fig. S6). In a second, slightly modified set of MC calculations, the cell concentration data of *L. danicus* were forced to be included in each tested combination performed by the pseudo-random simulation (set 2; Supporting Information Fig. S6). The reason for considering set 2 is that the mass occurrence of this specific diatom taxon, by far the most abundant diatom species in the studied year (Fig. 2), coincided with the timing of the largest Ba/Ca_{shell} peak in cage and sediment shells and thus suggested to be directly related to the Ba enrichment in the shell. In agreement with simulations of set 1, the most suitable combination was detected for a potential time lag of 4–7 d (in the following referred to as "scenario 2" considering *L. faveolata*, *C. socialis*, *Chaetoceros curvisetus*, *T. belgicus*, and *L. danicus*; Fig. 3; Supporting Information Fig. S6). Because the obtained species-specific weighting factors were affected by the time lag that was artificially applied to each diatom species, various tested time lags produced slightly different outcomes (Supporting Information Fig. S6). In this study, the short time lag (i.e., in the expected range which was previously approximated between phytoplankton bloom and geochemical response; Fröhlich et al. 2022*a*) was exclusively used to determine the potential phytoplankton combination (with weighting factors) that best matched the Ba/Ca_{shell} profile. As depicted in Supporting Information Fig. S7, the daily amount of Ba that ended up in the bivalve varied considerably between specimens in the cage (maximum of 1.6 $\mu g\ d^{-1}$) and on the sediment (maximum of 3.6 $\mu g\ d^{-1}$). However, an almost equal amount of Ba in 1 L of ingested seawater was needed to trigger the formation of the largest Ba/Ca_{shell} peaks in early June (Supporting Information Fig. S7) for shells from the cage (approximately 23 $ng\ L^{-1}$) and the sediment (approximately 27 $ng\ L^{-1}$) after taking the shell growth and filtration rates into consideration. Following the approximations performed for scenario 1 (Fig. 3), the hypothetically calculated amount of Ba (*see* Fig. S2) ranged between 52 and 221 $fg\ cell^{-1}$ (for the diatom taxa *T. belgicus* and *C. socialis*, respectively). Based on the estimates of scenario 2, an adequate amount of phytoplankton-associated Ba was potentially abundant in the seawater if the diatom cells contained between 2 (*L. danicus*) and 194 (*C. socialis*) fg Ba $cell^{-1}$ (Fig. 3).

Mo in shells, seawater, dinoflagellate blooms, and aggregation events

Mo/Ca_{shell} profiles (Figs. 1B, 4) of the cage shells showed two episodes of elevated Mo content, that is, at 29 June ($0.08 \pm 0.01\ \mu mol\ mol^{-1}$) and 08 September ($0.07 \pm 0.02\ \mu mol\ mol^{-1}$). Peak heights were nearly identical between the three specimens and clearly stood out from the background (approximately $0.03 \pm 0.01\ \mu mol\ mol^{-1}$,

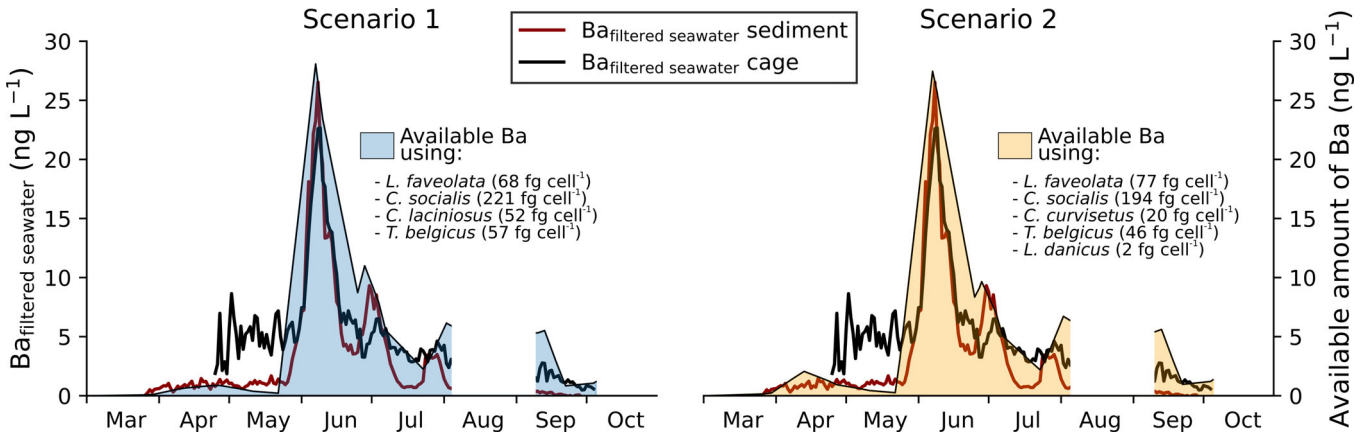

Fig. 3. Considering shell height, growth rates, and filtration rates (i.e., 5 L h^{-1} g^{-1} soft tissue dry weight), the $Ba_{filtered\ seawater}$ concentration was estimated from the Ba/Ca_{shell} profiles. Two potential diatom scenarios obtained by Monte Carlo simulations were used to estimate the diatom-associated amount of Ba following the assumption that the ingestion of diatoms triggered the formation of the Ba/Ca_{shell} peaks (*see* calculations described in the Supporting Information).

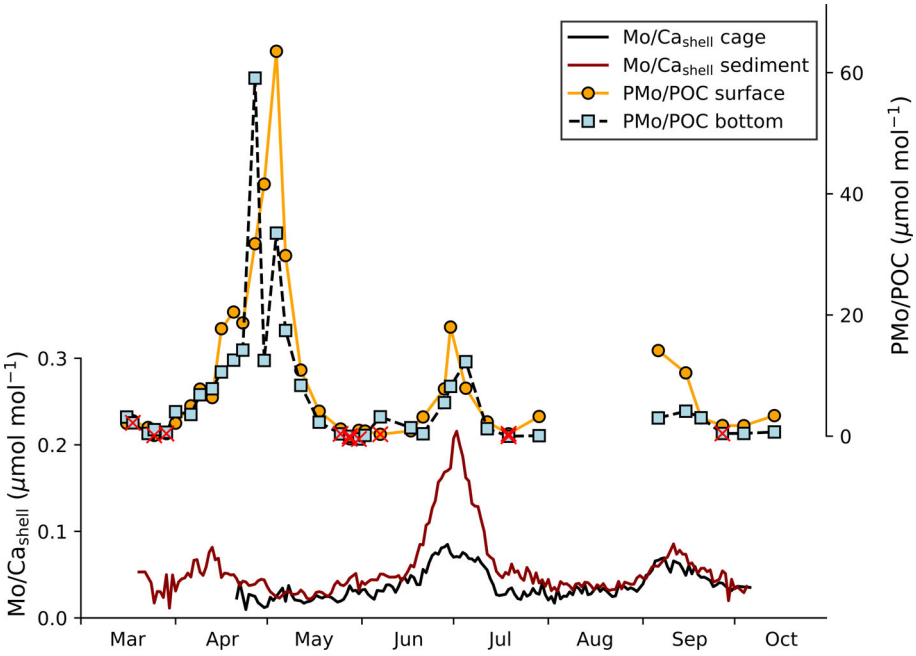

Fig. 4. Average Mo/Ca$_{shell}$ profiles from cage and sediment shells (from 2021) and the variation in PMo/POC ratios measured in surface and bottom waters. Note that some analyses of PMo remained below the limit of detection (indicated with a red cross).

Fig. 1B). In specimens from the sediment, a large Mo/Ca$_{shell}$ peak occurred at around the same time of the year (on 02 July) but was nearly threefold larger than in cage specimens (0.22 ± 0.09 μmol mol^{-1}, Fig. 1B). As in the cage shells, another Mo/Ca$_{shell}$ enrichment was observed in early September with an average magnitude of 0.09 ± 0.01 μmol mol^{-1}. Sediment specimens also revealed elevated Mo/Ca$_{shell}$ values (approximately 0.08 μmol mol^{-1}) in shell portions deposited in early April. The contemporaneous shell portions could not be studied in cage shells due to epibiont overgrowth. Sediment specimens contained, on average, 25% higher Mo/Ca$_{shell}$ values (0.04 ± 0.01 μmol mol^{-1}) than cage shells (Kruskal–Wallis test; $p < 0.001$, H[χ^2] = 74). The total (shell plus soft tissue) daily Mo incorporation ranged between 3 and 63 ng d^{-1} for cage specimens and 8 and 147 ng d^{-1} for sediment specimens (Fig. 5A). Considering the daily filtered water volume (Fig. 5A), Mo$_{filtered\ seawater}$ ranged between 0.03 to 0.78 ng Mo L^{-1} (Fig. 5B).

Levels of PMo/POC ratios likewise showed a flat baseline (note that low PMo/POC levels were slightly below the detection limit obtained for particulate Mo) with episodes of high PMo/POC levels (Fig. 4). In both bottom and surface waters, three PMo/POC events were observed in late April to early May (up to 59.10 and 63.53 μmol mol^{-1}, respectively), late June (reaching 12.29 and 18.01 μmol mol^{-1}, respectively), and early to mid-September (mainly occurring in surface water samples with ratios of 14.13 μmol mol^{-1}). Eight phytoplankton aggregation events were determined (V. Siebert unpubl.) to occur in the water column during 2021 (30 March; 12 and 27 April; 13 May; 06, 14, and 27 June; 02 October). Among these events, the aggregates observed in June showed notable enrichment in Mo (Fig. 5). The most abundant dinoflagellate species identified in 2021 belonged to the genus *Gymnodinium* with a maximum cell concentration of 33,440 cells L^{-1} on 04 May (V. Siebert unpubl.). More than half of these cells (68%) were smaller than 10 μm. Distinct blooms of this dinoflagellate occurred in early May, mid-June, and mid-September (Fig. 5B), contemporaneously with PMo/POC enrichments. Estimating the cellular Mo content (described in Discussion) of individual *Gymnodinium* spp. cells smaller than 10 μm (in length and diameter) yielded amounts of up to 500 fg cell^{-1} (Fig. 5C; *see* Discussion for calculations).

Li in shells and seawater

Cage and sediment shells revealed similar Li/Ca$_{shell}$ profiles (Fig. 1C) that were characterized by low values in early 2021 (on average, 32.65 ± 2.04 and 30.61 ± 3.71 μmol mol^{-1} until June in cage and sediment shells, respectively) and steadily increasing ratios during the main growing season in June and July (on average, 37.70 ± 3.35 μmol mol^{-1} in cage and 36.97 ± 2.98 μmol mol^{-1} in sediment specimens). Between August and mid-September, Li/Ca$_{shell}$ values were slightly higher in cage shells (49.20 ± 5.77 μmol mol^{-1}) than in sediment shells (45.40 ± 3.74 μmol mol^{-1}). Although no large, distinct peaks were observed in the Li/Ca$_{shell}$ chronologies (Fig. 1C), two smaller enrichment episodes were present during late summer (August to mid-September), with average values reaching 58.20–64.18 μmol mol^{-1} in cage shells and

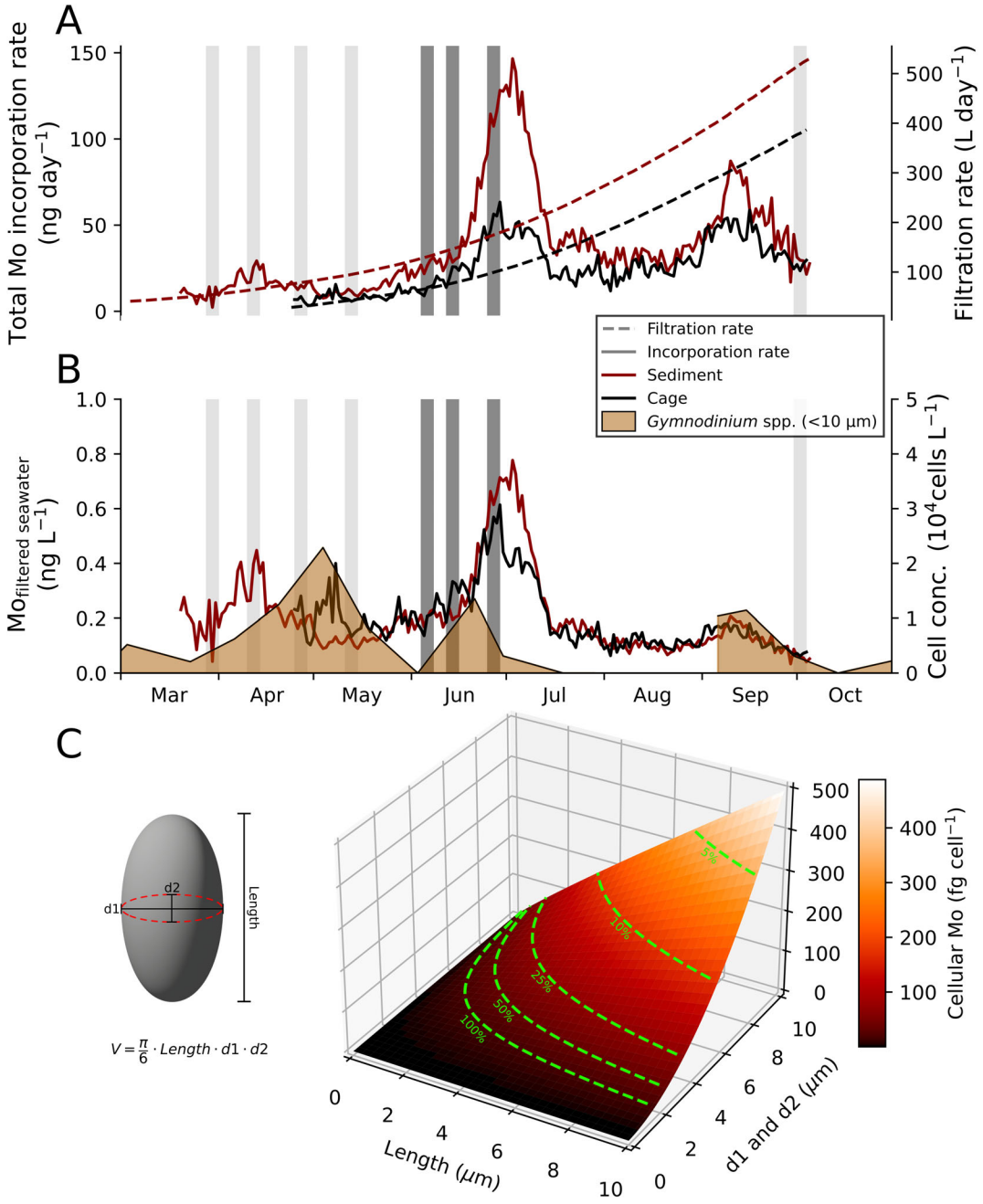

Fig. 5. Approximated total Mo incorporation rate into the scallops and filtration rate (at 5 L h^{-1} g^{-1} of soft tissue dry weight) for cage and sediment shells (**A**). The Mo$_{filtered\ seawater}$ concentration (based on the total Mo incorporation rate, growth, and filtration rate) and the temporal dynamics of the dominant dinoflagellate *Gymnodinium* spp. monitored at the study site (**B**). Periods of aggregate formation (determined by V. Siebert unpubl.) are indicated as light gray, vertical bars (**A** and **B**). Dark gray bars depict aggregation episodes during which significant loads of Mo were transported from the water column toward the SWI (V. Siebert unpubl.). The cellular Mo content at various cell volumes (**C**) was estimated using the cell geometry for *Gymnodinium* (Hillebrand et al. 1999; Sun and Liu 2003), the volume-to-carbon relationship for dinoflagellates (Menden-Deuer and Lessard 2000) and the elemental Mo/P (phosphorous) and C/P composition determined for the dinoflagellate *Gymnodinium chlorophorum* (Ho et al. 2003). The green graphs in the three-dimensional plot (**C**) illustrate potential values for cell parameters (if 100%, 50%, 25%, 10%, or 5% of the *Gymnodinium* spp. cells per liter were ingested by the scallops) that are required to provide an adequate amount of cellular Mo to meet the trace element requirement in the ingested seawater (estimated in **B**) to explain the observed Mo/Ca$_{shell}$ peaks.

50.73–52.99 μmol mol^{-1} in sediment shells. Until the end of shell growth in early October, Li/Ca$_{shell}$ ratios decreased rapidly in both groups (cage: 40.51 μmol mol^{-1}, sediment: 31.52 μmol mol^{-1}). Li/Ca$_{shell}$ data differed significantly between cage and sediment shells (Kruskal–Wallis test, $p < 0.05$, H[χ^2] = 6.0). It is noteworthy that similar results were

obtained after removing the estimated background signal from the measured Li/Ca_{shell} data.

Ratios of PLi to POC exhibited values ranging between 1.15 and 1289.74 in bottom and surface waters (Fig. 6). Aside from a large PLi/POC peak in March, two additional enrichments occurred in bottom PLi/POC ratios on 07 June (656.47 μmol mol^{-1}) and 15 September (384.88 μmol mol^{-1}). The latter coincided with the maximum PLi/POC ratio in surface waters.

Discussion

Ba/Ca_{shell} profiles

The synchronicity of the Ba/Ca_{shell} peaks (in cage and sediment specimens) and PBa/POC ratios of the water column (Fig. 2) suggests that shell Ba enrichments likely originated from the particulate phase (PBa), which is derived from the ambient water rather than the sediment. This finding corroborates the hypothesized trophic uptake of Ba-enriched suspended particles by scallop shells (e.g., Gillikin et al. 2008; Barats et al. 2009; Tabouret et al. 2012) that either originate from Ba accumulated on phytoplankton cell walls (Sternberg et al. 2005) or from enhanced barite precipitation (during the decay of phytoplankton blooms or the presence of acantharians in the water column) (e.g., Bishop 1988; Ganeshram et al. 2003). Direct ingestion of cellular Ba from living phytoplankton cells provides a reasonable explanation for elevated shell Ba levels because Ba/Ca_{shell} peaks occur simultaneously with blooms of certain diatom species and a strong increase in the PBa/POC ratio in early June (Fig. 2). This agrees to previous findings demonstrating that the occurrence of Ba/Ca_{shell} peaks is linked to the formation of phytoplankton blooms (i.e., mainly diatom blooms) (Thébault et al. 2009*a*; Fröhlich et al. 2022*a*,*b*). During the blooms, dissolved Ba from the ambient water is adsorbed onto phytoplankton cell walls (Sternberg et al. 2005) and the ingestion of those Ba-enriched cells by scallops leads to an elevated Ba concentration in the shell calcite after a few days. The hypothesis is further substantiated by a negative correlation between dissolved Ba and PBa in the seawater (V. Siebert unpubl.). While large phytoplankton blooms generate microenvironments facilitating the precipitation of barite (e.g., Dehairs et al. 1980; Bishop 1988), the ingestion of such particles could not sufficiently explain the formation of Ba/Ca_{shell} peaks in the scallop, *Comptopallium radula* (Thébault et al. 2009*a*). Moreover, the ingestion of rapidly sinking barite particles in decaying phytoplankton (Stecher and Kogut 1999) would have caused a larger Ba uptake by sediment specimens than by cage specimens because of the accumulation of large amounts of barite crystals at the SWI. However, after removing the influence of shell precipitation and filtration rates on the Ba/Ca_{shell} peaks, the $Ba_{filtered\ seawater}$ was nearly identical between cage and sediment shells (*see* Supporting Information Fig. S7), indicating that barite ingestion played only a minor role in the formation of shell Ba enrichments. Although the development of barite particles potentially contributed to the observed enrichments of PBa/POC in the water column, a pathway via barite uptake leading to the formation of the observed Ba/Ca_{shell} peaks in cage and sediment shells is less likely.

Consistent with previous findings (e.g., Barats et al. 2009; Fröhlich et al. 2022*b*), the variation in bulk phytoplankton or gross diatom abundance (Fig. 2) provided no striking similarities to the Ba/Ca_{shell} chronologies within the studied year (except the large peak in early June), reinforcing the assumption that phytoplankton or diatoms as a whole cannot explain the variability of Ba/Ca_{shell} peaks. This complicates the applicability of Ba/Ca_{shell} as a direct paleoproductivity proxy. The quantity of cell-associated Ba varies significantly between different phytoplankton species (Roth and Riley 1971; Fisher et al. 1991), indicating that the ingestion of some phytoplankton taxa contributes more to the measured Ba/Ca_{shell} peaks than other species (Fröhlich et al. 2022*b*). The pseudo-random MC calculations (considering species-specific amounts of cell-associated Ba) returned two possible scenarios (Fig. 3), which qualitatively illustrated that the dynamics of only four (scenario 1; Fig. 3) or five (scenario 2; Fig. 3) diatom species are sufficient to explain the observed Ba/Ca_{shell} patterns. Although both scenarios include chain-forming diatoms (i.e., *C. socialis* and *L. danicus*), which can potentially inhibit the shell growth of scallops due to gill clogging (Chauvaud et al. 1998; Lorrain et al. 2000), these diatom species cannot be excluded as potential food sources because no distinct reductions in growth rate (details about growth rates are provided in the Supporting Information) were observed during the formation of Ba/Ca_{shell} peaks. Aside from the diatom genus *Chaetoceros*, a well-known dietary component of *P. maximus* (e.g., Laing 2004), no further information about feeding preference or gut content was available for the studied scallops. Therefore, none of the potential diatom scenarios can be ruled out. Moreover, the small discrepancy in the estimated time lag (4–7 d; Supporting Information Fig. S6B) compared to the previously reported delay between phytoplankton blooms and geochemical response in the Ba/Ca_{shell} profiles (8–12 d; Fröhlich et al. 2022*a*,*b*) were most likely due to the low temporal resolution of the phytoplankton record and small uncertainties in the temporal alignment of the geochemical data. In fact, species-specific Ba loads between 2 and 221 fg cell^{-1} were estimated for the selected diatom species (Fig. 3), which fall in the range of cellular Ba content in different marine phytoplankton species (up to 245 fg cell^{-1}; Fisher et al. 1991). In particular, a cell-associated Ba load of 60 fg cell^{-1} can be approximated for *Chaetoceros* (using an average Ba concentration of 75.33 μg g^{-1} of dry weight [Lobus et al. 2021] at a maximum cellular dry weight for *C. gracilis* of approximately 0.8 ng cell^{-1} [Tachihana et al. 2020]), which is notably consistent with the cellular Ba range computed in the present study. Such combinations of qualitative and quantitative approaches provide ecologically reasonable estimates and suggest that the cell abundance of only a few diatom species containing a reasonable amount

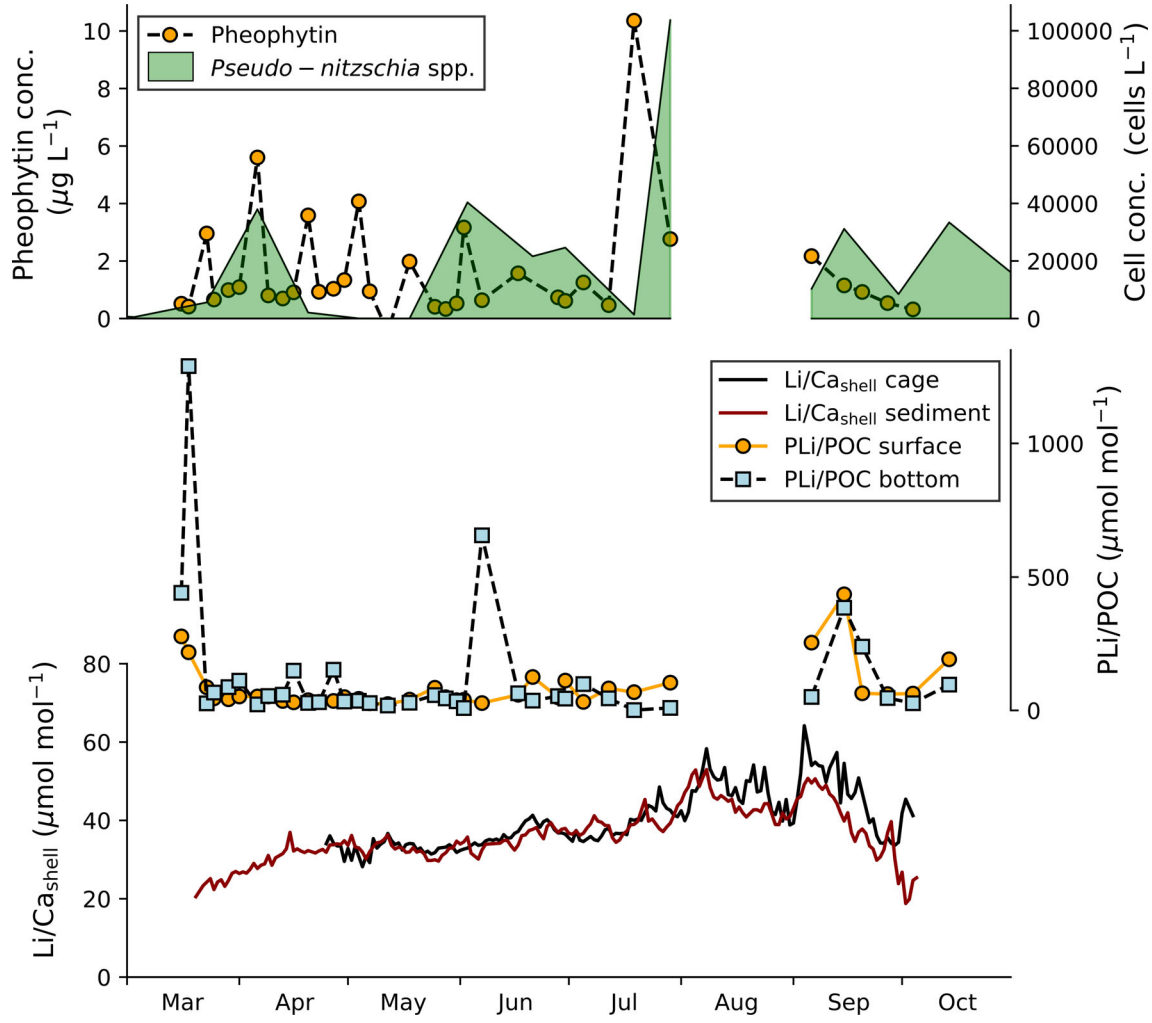

Fig. 6. Cell concentration time series of the diatom *Pseudo-nitzschia* spp. and pheophytin pigment concentration in 2021. Temporal variation of PLi/POC recorded in surface and bottom waters with averaged Li/Ca_{shell} profiles measured in cage and sediment shells.

of Ba can induce the formation of maxima in the Ba/Ca_{shell} chronology of *P. maximus*.

Interestingly, the significant difference in peak magnitudes of the elemental Ba/Ca_{shell} ratios between cage and sediment shells in early June (Fig. 2) was diminished after converting Ba/Ca_{shell} profiles to $Ba_{filtered\ seawater}$ (Fig. 3; Supporting Information Fig. S7). This suggests that the filtered seawater for both cage and sediment scallops contained nearly the same amount of Ba (during the formation of Ba/Ca_{shell} peaks), which could be induced by a diatom bloom in the ambient water. The higher Ba/Ca_{shell} peaks of sediment shells, on the other hand, seem to be mainly controlled by higher filtration and shell precipitation rates (Supporting Information Fig. S7). Aside from the difference in the averaged Ba/Ca_{shell} ratios of cage and sediment shells, a relatively large inter-specimen variation existed in the Ba/Ca_{shell} peak heights among sediment shells (i.e., the most distinct difference occurred between Shell D and Shell E in early June during the formation of the largest Ba/Ca_{shell} peak with 3.1 times higher values measured in Shell D; Supporting Information Fig. S4A). By computing the $Ba_{filtered\ seawater}$ contents for Shell D and Shell E according to their individual growth rate and filtration rate, this in situ measured Ba/Ca_{shell} discrepancy became less pronounced and differed by around 16 ng L^{-1} (1.7 times higher in Shell D compared to Shell E; Supporting Information Fig. S8). Nevertheless, it needs to be noted that an equal weight-standardized filtration rate of 5 L h^{-1} g^{-1} was considered for the calculation of $Ba_{filtered\ seawater}$ of Shell D and Shell E. Given that asynchronous, short-term changes in individual filtration activities were observed for scallops cultured in the same tank with identical conditions (Strohmeier et al. 2009), it is likely that individual variations in filtration rate might have induced such differences in peak heights. Alternatively, if the same amount of Ba (i.e., $Ba_{filtered\ seawater}$) was available in the water for Shell D and Shell E in early June, the filtration rate should have been slightly higher in Shell D to explain the larger

Ba/Ca_{shell} peak magnitude (e.g., given a scenario in which Shell D possessed a higher, yet realistic, relative filtration rate of about 8.6 L h^{-1} g^{-1} instead of 5 L h^{-1} g^{-1}, both specimens exhibited similar $Ba_{filtered\ seawater}$ levels; Supporting Information Fig. S8). Therefore, small individual differences in growth rate and filtration rate can result in significant differences in the measured Ba/Ca_{shell} profiles, which could affect the inter-specimen reproducibility of Ba/Ca_{shell} profiles. These findings suggest to adjust elemental Ba/Ca_{shell} ratios measured in *P. maximus* for filtration rate and shell growth rate before the data can be used as a potential quantitative indicator of past phytoplankton dynamics. Additional information about uncertainties in the estimations applied in this study is provided in the Supporting Information.

The Ba/Ca_{shell} background level of cage shells was significantly higher than that of sediment shells (Fig. 1A), even after approximating the $Ba_{filtered\ seawater}$ content (Fig. 3). This finding is potentially coupled to the observation of higher growth rates measured in cage-grown specimens (Supporting Information Fig. S3), a phenomenon previously reported for other scallop taxa, for example, *Crassadoma gigantea* (Leighton 1979), *Placopecten magellanicus* (MacDonald 1986), and *Lyropecten nodosus* (Mendoza et al. 2003). The higher growth rate in cage-grown scallops may be primarily associated with higher food availability (MacDonald 1986) because the cage was placed within the water column where bivalves potentially had better access to living planktonic organisms, such as diatoms. Thus, the constant provision of Ba-containing cells, selectively retained by scallop gills (Shumway et al. 1997; Beninger et al. 2004), potentially led to elevated Ba/Ca_{shell} background levels. Sediment particles within the digestive tract of scallops from the sediment (as reported by Shumway et al. 1987) could also affect the bivalves to efficiently assimilate their food, altering the gut pH and/or the retention time of food particles in the gut (e.g., Wang et al. 1995). This potential influence might have contributed to the observed differences in Ba/Ca_{shell} background, yet it needs to be confirmed in future studies by analyzing the gut content of scallops. The high variability in the Ba/Ca_{shell} profiles observed in cage shells compared to the more stable Ba/Ca_{shell} background measured in sediment shells (Fig. 1A) could be related to enhanced competition for resources between the cage scallops, given the high specimen density in the cage and the fact that scallops were reported to actively avoid high spatial population densities (e.g., MacDonald and Bajdik 1992). An inter-species food competition for cage scallops is also likely, as a large number of naturally growing, filter-feeding ascidians colonized the cage. Accordingly, scallops living on the sediment surface may have had limited access to large amounts of planktonic diatoms, but rather fed on a mixture of detritus and benthic microalgae. After phytoplankton bloom events, the decaying cells sank toward the SWI, where they got ingested by the scallops and triggered the formation of Ba/Ca_{shell}, peaks provided that the quantity of cellular Ba together with the cell abundance in the water was sufficient to cause a respective enrichment in the shells. Although it remains unknown to which extent the various factors (i.e., growth and filtration rates, food availability, resource competition, the spatial distribution of food, and phytoplankton dynamics) contributed to the observed differences in cage and sediment Ba/Ca_{shell} background levels, the findings indicate that *P. maximus* sensitively reacted to changes in their direct environment which subsequently affected the Ba/Ca_{shell} ratios.

Mo/Ca_{shell} profiles

Similar to Ba/Ca_{shell} profiles, the Mo/Ca_{shell} profiles of cage and sediment shells shared a remarkably similar pattern with the PMo/POC data recorded in the water column with three contemporaneous episodes of Mo enrichment (Fig. 4). This observation supports the assumption that shell Mo originates from the particulate phase (PMo) (Tabouret et al. 2012; Thébault et al. 2022). However, the magnitude of PMo/POC elevations (e.g., during late April to early May) does not correspond to the patterns measured in the Mo/Ca_{shell} profiles, suggesting that the scallops seem to have incorporated a non-proportionate amount of Mo from the PMo pool. Interestingly, after accounting for filtration (Fig. 5A) and shell growth rate, an episode of enhanced Mo concentration in the water ($Mo_{filtered\ seawater}$) was identified for cage shells in late April to early May (Fig. 5B), which was not obvious from the original Mo/Ca_{shell} profile (Fig. 4). This $Mo_{filtered\ seawater}$ enrichment exhibited very similar levels to that determined for sediment shells in April. Although a temporal offset exists, it can be assumed that the enhanced $Mo_{filtered\ seawater}$ concentrations for both cage and sediment shells were potentially induced by the same external event that occurred in the water column. The short temporal discrepancy between $Mo_{filtered\ seawater}$ of cage and sediment shells during this period (late April to early May) is likely an artifact of uncertainties in the absolute temporal alignment of the geochemical data (especially in growth increments closer to the first winter growth cessation). Furthermore, the approximation of $Mo_{filtered\ seawater}$ indicates that a comparable quantity of Mo was filtered from the ingested water by cage and sediment shells in early July, making the distinctively lower Mo/Ca_{shell} peak magnitudes in cage shells less pronounced (Fig. 5B). Following previous observations, Mo/Ca_{shell} peaks in scallops (*P. maximus* and *C. radula*) are associated with transport of Mo-enriched biogenic particles toward the SWI where they got ingested by the bivalves (Thébault et al. 2009*a*; Barats et al. 2010). More specifically, stressed phytoplankton cells (e.g., due to nutrient limitation, Toullec et al. 2021, or grazing by zooplankton, Toullec et al. 2019) tend to stick together, forming large particles, such as aggregates (e.g., Alldredge and Gotschalk 1988, 1989), which were proposed to sequester Mo from the dissolved phase (Dellwig et al. 2007; Mori et al. 2021) and induce Mo/Ca_{shell} peaks after digestion by the scallops (Thébault et al. 2009*a*, 2022). Siebert et al. (V. Siebert unpubl.) identified

multiple episodes of aggregate formations in the water column throughout the studied year (Fig. 5A,B; gray bars) and concluded that not all aggregation episodes were linked to a significant transport of PMo toward the SWI, but only three aggregation events in June were associated with an enhanced PMo transfer (Fig. 5A,B; dark gray bars). Accordingly, the largest Mo/Ca_{shell} peak observed in both sediment and cage shells occurred shortly after those three Mo-associated aggregation episodes (Figs. 4, 5), substantiating the aforementioned relationship between scallops and potentially ingested aggregates. However, the two remaining Mo/Ca_{shell} enrichments in April and September did not occur contemporaneously with aggregation events (Figs. 4, 5). Since the phytoplankton genus *Gymnodinium* is naturally enriched in Mo (Ho et al. 2003) and the most dominant dinoflagellate genus of the studied year, a large bloom event may have contributed to an excessive transfer of Mo from the dissolved phase to the particulate phase, which potentially accounted for the large PMo/POC ratio measured in early May (V. Siebert unpubl.). Compelling synchronicity in early May and September existed between the timing and magnitude of blooms of this dinoflagellate taxon (i.e., *Gymnodinium* spp. from the size fraction $< 10\ \mu m$) and the variation of enhanced $Mo_{filtered\ seawater}$ levels estimated for cage and sediment scallops (Fig. 5B). This is in agreement with the findings by Fröhlich et al. (2022*a*) reporting qualitative similarities in the occurrence of small cells ($< 20\ \mu m$) of the dinoflagellate *Gymnodinium* spp. and peaks in Mo/Ca_{shell} profiles of scallop shells from three studied years. Aside from the blooms of *Gymnodinium* spp. in early May and September, a third mass occurrence of this dinoflagellate developed in June, shortly before the largest shell Mo enrichment observed in this year (Fig. 5B). Similar to Ba/Ca_{shell}, a short time lag of a few days existed between a *Gymnodinium* spp. bloom and a Mo/Ca_{shell} peak (Fröhlich et al. 2022*a*), but this appears to be negligible given the uncertainties in absolute dating of the shell data and the low temporal resolution of phytoplankton monitoring. Assuming a linear relationship between cell abundance and Mo uptake, the cell concentration of *Gymnodinium* spp. during this bloom would have resembled the approximated $Mo_{filtered\ seawater}$ contents, which was not observed in this study. As described above, it is therefore likely that episodes of aggregate formation observed in June resulted in loads of PMo transported toward the SWI (Dellwig et al. 2007). Furthermore, the retention of small aggregate particles (Thébault et al. 2022), in addition to the ingestion of Mo-enriched cells of *Gymnodinium* spp., led to an enhanced Mo uptake by the scallops. The contemporaneity of *Gymnodinium* spp. blooms and phytoplankton aggregation may represent an allelopathic relationship (i.e., one organism produced biochemical compounds affecting the growth or survival of another) between dinoflagellates and other phytoplankton taxa. The allelopathic relation may have stressed the phytoplankton in competition with the dominant *Gymnodinium* genus (e.g., Kubanek et al. 2005). Such stress may either induce cell lysis or promote the excretion of large amounts of sticky polymers, both mechanisms triggering the aggregation of phytoplankton cells. The small difference in the $Mo_{filtered\ seawater}$ concentration between cage and sediment shells in early July (Fig. 5B) could be a result of aggregate particles that sank rapidly toward the SWI and resided shortly in the water column, making them more available to scallops living on the sediment surface. This hypothesis can hardly be validated in the current study because the estimations contain several uncertainties (*see* Supporting Information) that potentially contributed to differences in the absolute trace element uptake. However, these findings confirm that the patterns in Mo/Ca_{shell} profiles are potentially influenced by phytoplankton dynamics within the water column, where both *Gymnodinium* spp. blooms and aggregation events play a role in Mo/Ca_{shell} peak formation.

Based on the hypothesis that the formation of Mo/Ca_{shell} peaks can be triggered by the ingestion of small *Gymnodinium* spp. cells ($< 10\ \mu m$), the intracellular Mo content of this dinoflagellate was estimated to evaluate if this pathway can provide a sufficient load of PMo to explain respective trace element enrichments in the scallop shells. Unlike most phytoplankton (e.g., Morris and Syrett 1963; Eppley et al. 1969), this dinoflagellate is inferred to potentially use nitrate instead of ammonium for nitrogen assimilation (Yamamoto et al. 2004). The utilization of nitrate requires the synthesis of the Mo-containing enzyme nitrate reductase (Collier 1985; Marino et al. 2003), which could be the cause for the enhanced Mo content observed in *Gymnodinium* cells (Fröhlich et al. 2022*a*). Ho et al. (2003) determined the element ratios of Mo and carbon (C), both normalized to phosphorus (P), in the dinoflagellate species *Gymnodinium chlorophorum*, suggesting a molar Mo/C ratio of 0.8 mmol mol^{-1} (using Mo/P of 0.11 mol mol^{-1} and C/P of 137 mol mol^{-1}). An empirical relationship between carbon content and cell volume was defined for dinoflagellates (pg C $cell^{-1} = 0.216 \times volume^{0.939}$; Menden-Deuer and Lessard 2000), where the cell volume can be estimated by a geometric model for *Gymnodinium* cells (Fig. 5C; Hillebrand et al. 1999; Sun and Liu 2003). These features allowed to estimate the range of absolute cellular Mo content at various possibilities in the shape of *Gymnodinium* cells (i.e., length, diameter d1 and d2; Fig. 5C). Considering that the total pool of *Gymnodinium* cells within each liter of filtered seawater was retained by the scallops, a cellular Mo load of 17.5 fg $cell^{-1}$ (Fig. 5C; green 100% graph) was calculated (e.g., 0.4 ng Mo L^{-1} of filtered water at 22,880 cells L^{-1} in early May; Fig. 5B). Based on the above-described cell geometry-to-Mo content relationship, the *Gymnodinium* cell volumes would have been about 14.7 μm^3, considering a cell length of 7 μm and a diameter of 2 μm for d1 and d2 (Fig. 5C), which agrees with the observed phytoplankton in this study (a length of $< 10\ \mu m$ of the recorded *Gymnodinium* spp. cells). Given that many species of *Gymnodinium* have been reported toxic and could hamper shell growth in bivalves (Widdows et al. 1979;

Chauvaud et al. 2001), cells of *Gymnodinium* are likely not the preferred diet of *P. maximus* and only ingested by smaller amounts. In fact, a reduction in growth rate was observed for sediment scallops during the first large *Gymnodinium* bloom in early May (Supporting Information Fig. S3). Therefore, a scenario in which only 5% of the total *Gymnodinium* spp. cells were ingested (i.e., corresponding to a cell concentration as low as 1144 cells L^{-1} in early May) is likely, which would result in a cellular Mo load of up to 349.7 fg $cell^{-1}$ to account for the estimated $Mo_{filtered\ seawater}$ requirement of 0.4 ng Mo L^{-1} for the cage and sediment shells (in early May). Interestingly, even this high cellular Mo content can be contained in *Gymnodinium* cells with a length and diameter not exceeding 10 μm (e.g., at a length of 8.4 and 9 μm in diameter d1 and d2; Fig. 5C; green 5% graph). In other words, the ingestion of cells of only a very small portion (< 5%) of the total *Gymnodinium* spp. (< 10 μm) pool provided a sufficient concentration of $Mo_{filtered\ seawater}$ to induce the formation of the Mo/Ca_{shell} peaks in the cage and sediment shells. Although these calculations were based on multiple assumptions, this line of evidence supports that a potential link exists between the dinoflagellate genus *Gymnodinium* and Mo/Ca_{shell} peaks. Despite the fact that ammonium assimilating diatoms leading to the formation of Ba/Ca_{shell} peaks are assumed to contain only low amounts of cellular Mo (repressed synthesis of the Mo-containing enzyme nitrate reductase), such diatom blooms could have eventually contributed slightly to the large Mo/Ca_{shell} peak during summer. To investigate the impact of various phytoplankton taxa cultivated using different nitrogen sources on the Mo content in scallop shells, future studies should incorporate feeding experiments. These experiments will provide valuable insights into the relationship between phytoplankton composition and nitrogen sources in relation to Mo accumulation in scallop shells.

Despite small differences observed in the Mo/Ca_{shell} background levels (Fig. 1B), after accounting for growth and filtration rates (Fig. 5A), the $Mo_{filtered\ seawater}$ concentration revealed closely similar levels between cage and sediment shells outside Mo enrichment episodes (Fig. 5B). Compared to the significant deviations in the Ba/Ca_{shell} background levels that can be explained by small differences in the ambient environment of the scallops, the more similar Mo requirements in cage and sediment shells suggest that such small environmental variations did not affect Mo/Ca_{shell} background levels. Instead, only during distinct events in the water column (e.g., aggregation episodes and/or large dinoflagellate blooms), enhanced loads of Mo enter the scallops and lead to the formation of Mo/Ca_{shell} peaks. This is in agreement with previous findings showing that the digestive gland is the most Mo-enriched organ (about 69% of the total shell Mo content; Barats et al. 2010; Thébault et al. 2022) and that variations of dissolved Mo in seawater contribute insignificantly to the Mo/Ca_{shell} profiles (Barats et al. 2010; Tabouret et al. 2012).

Li/Ca_{shell} profiles

Unlike past Li/Ca_{shell} chronologies of *P. maximus*, respective profiles of cage and sediment specimens in the present study did not show large and distinct peaks (e.g., a Li/Ca_{shell} peak of approximately 159 μmol mol^{-1} was measured in scallops by Thébault et al. 2022). However, two small Li/Ca_{shell} enrichments in August and September occurred contemporaneously in cage and sediment shells (Fig. 6). These Li enrichments were even more pronounced when converted to an absolute daily Li incorporation rate (Supporting Information Fig. S9), using the relationship between daily shell growth rates and the Li/Ca_{shell} background (Thébault and Chauvaud 2013) together with the daily Ca precipitation rate (Supporting Information Fig. S2). This indicates a common environmental forcing acting upon Li incorporation into the shells. It was previously hypothesized that Li from the dissolved phase is removed by the production of biogenic opal (Coplen et al. 2002) in diatom frustules that can lead to the transport of large quantities of Li toward the SWI, triggering the formation of Li/Ca_{shell} peaks in scallops (Thébault and Chauvaud 2013; Thébault et al. 2022). The large diatom blooms in early June and mid-September (Fig. 2) occurred contemporaneously with increased PLi/POC levels in bottom waters, while increased PLi/POC values were only detected at the surface water in mid-September (Fig. 6). The latter PLi/POC event (September) also coincided with a Li/Ca_{shell} enrichment, corroborating a link between diatom abundance and shell Li enrichments. However, no respective Li/Ca_{shell} peak occurred in June after the formation of the largest diatom bloom (Fig. 2). A possible explanation for the absence of a respective Li/Ca_{shell} enrichment in early June is that either particulate Li was associated with a diatom species that was not ingested by the scallops or another process was involved that caused the recorded peak in PLi/POC at the SWI, such as the resuspension of Li-enriched sediment particles (Tardy et al. 1972) that were not filtered and retained by the scallops. Alternatively, Thébault et al. (2022) demonstrated that after large diatom blooms, the recycling of biogenic silica at the SWI also releases frustule-associated Li into the ambient water, causing distinct Li/Ca_{shell} peaks in scallops. The lack of a Li/Ca_{shell} peak following the large diatom bloom in June could potentially be linked to the observation that a large number of epifaunal brittlestars, *Ophiocomina nigra*, colonized the seabed. This omnivorous echinoderm species could have consumed most of the organic-enriched particles at the SWI, including deposited diatom frustules, which, in turn, prohibited the dissolution of Li into the water column. Unfortunately, no environmental monitoring data are available for August during the formation of the first small Li/Ca_{shell} enrichment to further constrain these links.

Another proposed hypothesis describes a potential relationship between the diatom genus *Pseudo-nitzschia* spp. and the formation of transient Li/Ca_{shell} peaks in *P. maximus* (Thébault and Chauvaud 2013; Fröhlich et al. 2022*a*). Under

stressful conditions, such as nutrient limitations and/or enhanced predatory activity by zooplankton (Pan et al. 1996; Bates et al. 2018), *Pseudo-nitzschia* spp. cells produce the neurotoxin domoic acid which requires the presence of intracellular Li (Subba Rao et al. 1998). The ingestion of those cells by scallops can lead to elevated Li/Ca_{shell} levels. In the studied year, several *Pseudo-nitzschia* spp. blooms were recorded (Fig. 6), including large blooms in June, at the end of July (i.e., the most abundant diatom genus; Fig. 2), and in September. However, only during the end of July high concentrations of pheophytin pigments (an indicator for increased predation activity of zooplankton; Lorenzen 1967) were observed at the beginning of the development of a *Pseudo-nitzschia* spp. bloom (Fig. 6), generating conditions for this diatom to produce the Li-associated neurotoxin. Considering a short time lag between the timing of the diatom bloom and the formation of Li/Ca_{shell} enrichments (cf. Fröhlich et al. 2022*a*), this pathway seems to provide a possible explanation for the Li enrichment in cage and sediments shells in August. A similar pattern occurred in September, during the presence of elevated pheophytin levels ($2\ \mu g\ L^{-1}$) and the development of a *Pseudo-nitzschia* spp. bloom (Fig. 6). This may have induced the formation of the second episode of elevated Li/Ca_{shell}. However, as blooms of this diatom also occurred prior to the two Li/Ca_{shell} enrichment episodes (i.e., in April and June) at slightly increased pheophytin pigment concentrations (Fig. 6), the absence of respective trace element peaks in the scallop shells argues against the proposed link. The observed discrepancies may be explained by a species-specific filtration of scallops because these blooms were composed of different *Pseudo-nitzschia* species.

The exact uptake mechanisms of Li from the water column to the incorporation into the scallop shells need to be further validated by a longer time series of Li/Ca_{shell} and environmental records. Nonetheless, the hypotheses of Li formation in scallop shells discussed in this study may also apply to the formation of larger, distinct Li/Ca_{shell} peaks (e.g., Thébault et al. 2022), making Li/Ca_{shell} chronologies a geochemical proxy for recording short-term changes in the water column. A reliable estimation of the absolute amount of Li filtered from the water (like $Ba_{filtered\ seawater}$ and $Mo_{filtered\ seawater}$) could not be performed because no information about the relative distribution of this trace element in soft tissue and the shell was available. However, when considering differences in the volume of filtered seawater between cage and sediment specimens (Supporting Information Fig. S7), it can be estimated that scallops from the sediment filtered seawater that contained about 36% less Li relative to cage scallops during the Li enrichments in August and September (Supporting Information Fig. S9). Accordingly, Li potentially derived from planktonic particles which might have been more accessible to the cage scallops, analogous to the observation of the enhanced ingestion of Ba-enriched phytoplankton for cage shells.

Summary and conclusions

Shell Ba/Ca and Mo/Ca profiles of *P. maximus* differed among specimens grown on the seafloor and in a cage 1 m above the sediment–water interface. A close link existed between elements bound to organic particles in the water column and Ba/Ca_{shell} and Mo/Ca_{shell} data, supporting previously proposed hypotheses on the trophic uptake of those elements by scallops. Computing the trace element concentrations in the seawater filtered by the scallops using a novel model that combines element-to-calcium ratios with physiological parameters such as shell height, growth rates, and filtration rates showed that the theoretical filtered Ba and Mo loads in the seawater were nearly identical between sediment and cage scallops during Ba/Ca_{shell} and Mo/Ca_{shell} peak formation. The observed geochemical differences were rather related to growth conditions than different food or water conditions. The approximations obtained from the MC simulations indicated that the timing and magnitude of Ba/Ca_{shell} peaks can be quantitatively modeled by blooms of specific diatom species containing different amounts of cellular Ba. The Mo/Ca_{shell} profiles appeared to be related to the timing of Mo-enriched dinoflagellate species (*Gymnodinium* spp.) as well as to the occurrence of aggregate-forming diatoms transporting particulate Mo toward the SWI. Li/Ca_{shell} profiles did not show distinct peaks. However, two small Li enrichments occurred in all studied shells contemporaneously with elevated particulate Li concentration in the water, supporting assumptions according to which Li is derived not only from the dissolved phase but also from the particulate fraction. These findings add new insights into uptake mechanisms of Ba, Mo, and Li from the seawater into the shells of scallops, allowing further refined Ba/Ca_{shell}, Mo/Ca_{shell}, and Li/Ca_{shell} ratios as proxies for short-term phytoplankton dynamics. However, future studies should focus on the geochemical records of Li/Ca_{shell} ratios before considering their application as a potential phytoplankton proxy. As demonstrated herein, the strong influence of specimen-specific physiological parameters (filtration rate, growth rate, and shell height) on shell chemistry highlights the necessity to adjust element chemical data before they can serve as quantitative paleoenvironment proxies. Since each element alone suggests to be a potential indicator for phytoplankton dynamics, future studies might also focus on determining whether the combination of all three elements in a multi-proxy approach can be effective and what additional information about marine biogeochemical cycles can be derived from it.

Data availability statement

The data used and analyzed in this study are published in Siebert et al. (2023) and available at the SEANOE data repository (https://www.seanoe.org/data/00808/92043/). All additional supporting materials are provided in the Supporting Information.

References

Alldredge, A. L., and C. Gotschalk. 1988. In situ settling behavior of marine snow. Limnol. Oceanogr. **33**: 339–351. doi:10.4319/lo.1988.33.3.0339

Alldredge, A. L., and C. C. Gotschalk. 1989. Direct observations of the mass flocculation of diatom blooms: Characteristics, settling velocities and formation of diatom aggregates. Deep-Sea Res. I: Oceanogr. Res. Pap. **36**: 159–171. doi:10.1016/0198-0149(89)90131-3

Barats, A. 2006. Micro analyse quantitative des éléments traces dans la calcite de la coquille Saint Jacques (*Pecten maximus*) par Ablation Laser ICP-MS: une archive journalière de la biogéochimie des environnements côtiers tempérés. Diss. Université de Pau et des Pays de l'Adour.

Barats, A., D. Amouroux, L. Chauvaud, C. Pécheyran, A. Lorrain, J. Thébault, T. M. Church, and O. F. X. Donard. 2009. High frequency barium profiles in shells of the great scallop *Pecten maximus*: A methodical long-term and multi-site survey in Western Europe. Biogeosciences **6**: 157–170. doi:10.5194/bg-6-157-2009

Barats, A., D. Amouroux, C. Pécheyran, L. Chauvaud, J. Thébault, and O. F. X. Donard. 2010. Spring molybdenum enrichment in scallop shells: A potential tracer of diatom productivity in temperate coastal environments (Brittany, NW France). Biogeosciences **7**: 233–245. doi:10.5194/bg-7-233-2010

Barbier, E. B., S. D. Hacker, C. Kennedy, E. W. Koch, A. C. Stier, and B. R. Silliman. 2011. The value of estuarine and coastal ecosystem services. Ecological monographs **81**: 169–193. doi:10.1890/10-1510.1

Bates, S. S., K. A. Hubbard, N. Lundholm, M. Montresor, and C. P. Leaw. 2018. *Pseudo-nitzschia*, *Nitzschia*, and domoic acid: New research since 2011. Harmful Algae **79**: 3–43. doi:10.1016/j.hal.2018.06.001

Beninger, P. G., P. Decottignies, and Y. Rincé. 2004. Localization of qualitative particle selection sites in the heterorhabdic filibranch *Pecten maximus* (Bivalvia: Pectinidae). Mar. Ecol. Prog. Ser. **275**: 163–173. doi:10.3354/meps275163

Bishop, J. K. B. 1988. The barite-opal-organic carbon association in oceanic particulate matter. Nature **332**: 341–343. doi:10.1038/332341a0

Chauvaud, L., G. Thouzeau, and Y. M. Paulet. 1998. Effects of environmental factors on the daily growth rate of *Pecten maximus* juveniles in the Bay of Brest (France). J. Exp. Mar. Biol. Ecol. **227**: 83–111. doi:10.1016/S0022-0981(97)00263-3

Chauvaud, L., A. Donval, G. Thouzeau, Y. M. Paulet, and E. Nézan. 2001. Variations in food intake of *Pecten maximus* (L.) from the bay of Brest (France): Influence of environmental factors and phytoplankton species composition. C. R. Acad. Sci. III **324**: 743–755. doi:10.1016/S0764-4469(01)01349-X

Clark, G. R. 2005. Daily growth lines in some living Pectens (Mollusca: Bivalvia), and some applications in a fossil relative: Time and tide will tell. Palaeogeogr. Palaeoclimatol. Palaeoecol. **228**: 26–42. doi:10.1016/j.palaeo.2005.03.044

Collier, R. W. 1985. Molybdenum in the Northeast Pacific Ocean. Limnol. Oceanogr. **30**: 1351–1354. doi:10.4319/lo.1985.30.6.1351

Coplen, T. B., and others. 2002. Isotope-abundance variations of selected elements (IUPAC technical report). Pure Appl. Chem. **74**: 1987–2017. doi:10.1351/pac200274101987

Dehairs, F., R. Chesselet, and J. Jedwab. 1980. Discrete suspended particles of barite and the barium cycle in the open ocean. Earth Planet. Sci. Lett. **49**: 528–550. doi:10.1016/0012-821X(80)90094-1

Dellwig, O., M. Beck, A. Lemke, M. Lunau, K. Kolditz, B. Schnetger, and H. J. Brumsack. 2007. Non-conservative behaviour of molybdenum in coastal waters: Coupling geochemical, biological, and sedimentological processes. Geochim. Cosmochim. Acta **71**: 2745–2761. doi:10.1016/j.gca.2007.03.014

Eppley, R. W., J. L. Coatsworth, and L. Solórzano. 1969. Studies of nitrate reductase in marine phytoplankton. Limnol. Oceanogr. **14**: 194–205. doi:10.4319/lo.1969.14.2.0194

Field, C. B., M. J. Behrenfeld, J. T. Randerson, and P. Falkowski. 1998. Primary production of the biosphere: Integrating terrestrial and oceanic components. Science **281**: 237–240. doi:10.1126/science.281.5374.237

Fisher, N. S., R. R. L. Guillard, and D. C. Bankston. 1991. The accumulation of barium by marine phytoplankton grown in culture. J. Mar. Res. **49**: 339–354. doi:10.1357/002224091784995882

Fröhlich, L., V. Siebert, Q. Huang, J. Thébault, K. P. Jochum, and B. R. Schöne. 2022*a*. Deciphering the potential of Ba/Ca, Mo/Ca and Li/Ca profiles in the bivalve shell *Pecten maximus* as proxies for the reconstruction of phytoplankton dynamics. Ecol. Indic. **141**: 109121. doi:10.1016/j.ecolind.2022.109121

Fröhlich, L., V. Siebert, E. O. Walliser, J. Thébault, K. P. Jochum, L. Chauvaud, and B. R. Schöne. 2022*b*. Ba/Ca profiles in shells of *Pecten maximus*—A proxy for specific primary producers rather than bulk phytoplankton. Chem. Geol. **593**: 120743. doi:10.1016/J.CHEMGEO.2022.120743

Ganeshram, R. S., R. François, J. Commeau, and S. L. Brown-Leger. 2003. An experimental investigation of barite formation in seawater. Geochim. Cosmochim. Acta **67**: 2599–2605. doi:10.1016/S0016-7037(03)00164-9

Gillikin, D. P., F. Dehairs, A. Lorrain, D. Steenmans, W. Baeyens, and L. André. 2006. Barium uptake into the shells of the common mussel (*Mytilus edulis*) and the potential for estuarine paleo-chemistry reconstruction. Geochim. Cosmochim. Acta **70**: 395–407. doi:10.1016/j.gca.2005.09.015

Gillikin, D. P., A. Lorrain, Y. M. Paulet, L. André, and F. Dehairs. 2008. Synchronous barium peaks in high-

resolution profiles of calcite and aragonite marine bivalve shells. Geo-Mar. Lett. **28**: 351–358. doi:10.1007/s00367-008-0111-9

Hallegraeff, G. M. 1993. A review of harmful algal blooms and their apparent global increase. Phycologia **32**: 79–99. doi:10.2216/i0031-8884-32-2-79.1

Hillebrand, H., C. D. Dürselen, D. Kirschtel, U. Pollingher, and T. Zohary. 1999. Biovolume calculation for pelagic and benthic microalgae. J. Phycol. **35**: 403–424. doi:10.1046/j.1529-8817.1999.3520403.x

Ho, T. Y., A. Quigg, Z. V. Finkel, A. J. Milligan, K. Wyman, P. G. Falkowski, and F. M. M. Morel. 2003. The elemental composition of some marine phytoplankton. J. Phycol. **39**: 1145–1159. doi:10.1111/j.0022-3646.2003.03-090.x

Iglesias-Rodriguez, M. D., and others. 2008. Phytoplankton calcification in a high-CO2 world. Science **320**: 336–340. doi:10.1126/science.1154122

Kubanek, J., M. K. Hicks, J. Naar, and T. A. Villareal. 2005. Does the red tide dinoflagellate *Karenia brevis* use allelopathy to outcompete other phytoplankton? Limnol. Oceanogr. **50**: 883–895. doi:10.4319/LO.2005.50.3.0883

Laing, I. 2004. Filtration of king scallops (*Pecten maximus*). Aquaculture **240**: 369–384. doi:10.1016/j.aquaculture.2004.02.002

Leighton, D. L. 1979. A growth profile for the rock scallop *Hinnites multirugosus* held at several depths off La Jolla, California. Mar. Biol. **51**: 229–232. doi:10.1007/BF00386802

Lewitus, A. J., and others. 2012. Harmful algal blooms along the north American west coast region: History, trends, causes, and impacts. Harmful Algae **19**: 133–159. doi:10.1016/J.HAL.2012.06.009

Lobus, N. v., M. S. Kulikovskiy, and Y. I. Maltsev. 2021. Multielement composition of diatom *Chaetoceros* spp. from natural phytoplankton assemblages of the Russian Arctic seas. Biology **10**: 1009. doi:10.3390/biology10101009

Lorenzen, C. J. 1967. Vertical distribution of chlorophyll and phaeo-pigments: Baja California. Deep-Sea Res. Oceanogr. Abstr. **14**: 735–745. doi:10.1016/S0011-7471(67)80010-X

Lorrain, A., Y. M. Paulet, L. Chauvaud, N. Savoye, E. Nézan, and L. Guérin. 2000. Growth anomalies in *Pecten maximus* from coastal waters (Bay of Brest, France): Relationship with diatom blooms. J. Mar. Biolog. Assoc. UK **80**: 667–673. doi:10.1017/S0025315400002496

Lorrain, A., Y. M. Paulet, L. Chauvaud, R. B. Dunbar, D. Mucciarone, and M. Fontugne. 2004. $\delta^{13}C$ variation in scallop shells: Increasing metabolic carbon contribution with body size? Geochim. Cosmochim. Acta **68**: 3509–3519. doi:10.1016/j.gca.2004.01.025

MacDonald, B. A. 1986. Production and resource partitioning in the giant scallop *Placopecten magellanicus* grown on the bottom and in suspended culture. Mar. Ecol. Progr. Ser. **34**: 79–86. doi:10.3354/meps034079

MacDonald, B. A., and C. D. Bajdik. 1992. Orientation and distribution of individual *Placopecten magellanicus* (Gmelin) in two natural populations with differing production. Can. J. Fish. Aquat. Sci. **49**: 2086–2092. doi:10.1139/f92-232

Marali, S., B. R. Schöne, R. Mertz-Kraus, S. M. Griffin, A. D. Wanamaker, P. G. Butler, H. A. Holland, and K. P. Jochum. 2017. Reproducibility of trace element time-series (Na/Ca, Mg/Ca, Mn/Ca, Sr/Ca, and Ba/Ca) within and between specimens of the bivalve *Arctica islandica*—A LA-ICP-MS line scan study. Palaeogeogr. Palaeoclimatol. Palaeoecol. **484**: 109–128. doi:10.1016/j.palaeo.2016.11.024

Marino, R., R. W. Howarth, F. Chan, J. J. Cole, and G. E. Likens. 2003. Sulfate inhibition of molybdenum-dependent nitrogen fixation by planktonic cyanobacteria under seawater conditions: A non-reversible effect. Hydrobiologia **500**: 277–293. doi:10.1023/A:1024641904568

Masuzawa, T., and others. 1999. Multielement compositions of marine phytoplankton samples from coastal areas of Japan by instrumental neutron activation analysis. Biol. Trace. Elem. Res. **71**: 331–342. doi:10.1007/BF02784220

McConnaughey, T. A., and D. P. Gillikin. 2008. Carbon isotopes in mollusk shell carbonates. Geo-Mar. Lett. **28**: 287–299. doi:10.1007/s00367-008-0116-4

Menden-Deuer, S., and E. J. Lessard. 2000. Carbon to volume relationships for dinoflagellates, diatoms, and other protist plankton. Limnol. Oceanogr. **45**: 569–579. doi:10.4319/LO.2000.45.3.0569

Mendoza, Y., L. Freites, C. J. Lodeiros, J. A. López, and J. H. Himmelman. 2003. Evaluation of biological and economical aspects of the culture of the scallop *Lyropecten* (*Nodipecten*) *nodosus* in suspended and bottom culture. Aquaculture **221**: 207–219. doi:10.1016/S0044-8486(02)00646-4

Mori, C., M. Beck, M. Striebel, J. Merder, B. Schnetger, T. Dittmar, K. Pahnke, and H. J. Brumsack. 2021. Biogeochemical cycling of molybdenum and thallium during a phytoplankton summer bloom: A mesocosm study. Mar. Chem. **229**: 103910. doi:10.1016/J.MARCHEM.2020.103910

Morris, I., and P. J. Syrett. 1963. The development of nitrate reductase in *Chlorella* and its repression by ammonium. Arch. Mikrobiol. **47**: 32–41. doi:10.1007/BF00408287

Palmer, R. E. 1980. Behavioral and rhythmic aspects of filtration in the bay scallop, *Argopecten irradians concentricus* (say), and the oyster, *Crassostrea virginica* (Gmelin). J. Exp. Mar. Biol. Ecol. **45**: 273–295. doi:10.1016/0022-0981(80)90062-3

Pan, Y., D. V. Subba Rao, K. H. Mann, R. G. Brown, and R. Pocklington. 1996. Effects of silicate limitation on production of domoic acid, a neurotoxin, by the diatom *Pseudo-nitzschia multiseries*. I. Batch culture studies. Mar. Ecol. Prog. Ser. **131**: 225–233. doi:10.3354/MEPS131225

Poppeschi, C., and others. 2022. Interannual variability of the initiation of the phytoplankton growing period in two French coastal ecosystems. Biogeosciences **19**: 5667–5687. doi:10.5194/bg-19-5667-2022

Richard, M. 2009. Analyse de la composition élémentaire de *Pecten maximus* par HR-ICP-MS Element 2: développements méthodologiques et interprétations écologiques. Diss. Université de Bretagne occidentale-Brest.

Roth, I., and J. P. Riley. 1971. The distribution of trace elements in some species of phytoplankton grown in culture. J. Mar. Biol. Assoc. UK **51**: 63–72. doi:10.1017/S0025315400006457

Schöne, B. R., K. Tanabe, D. L. Dettman, and S. Sato. 2003. Environmental controls on shell growth rates and $\delta^{18}O$ of the shallow-marine bivalve mollusk *Phacosoma japonicum* in Japan. Mar. Biol. **142**: 473–485. doi:10.1007/S00227-002-0970-Y

Schöne, B. R., X. Huang, M. L. Zettler, L. Zhao, R. Mertz-kraus, K. Peter, and E. O. Walliser. 2021. Mn/Ca in shells *of Arctica islandica* (Baltic Sea)—A potential proxy for ocean hypoxia? Estuar. Coast. Shelf Sci. **251**: 107257. doi:10.1016/j.ecss.2021.107257

Schöne, B. R., S. Marali, A. Jantschke, R. Mertz-Kraus, P. G. Butler, and L. Fröhlich. 2023. Can element chemical impurities in aragonitic shells of marine bivalves serve as proxies for environmental variability? Chem. Geol. **616**: 121215. doi:10.1016/J.CHEMGEO.2022.121215

Shumway, S. E., R. Selvin, and D. F. Schick. 1987. Food resources related to habitat in the scallop *Placopecten magellanicus*. J. Shellfish Res. **6**: 89–95.

Shumway, S. E., T. L. Cucci, M. P. Lesser, N. Bourne, and B. Bunting. 1997. Particle clearance and selection in three species of juvenile scallops. Aquacult. Int. **5**: 89–99. doi:10.1007/BF02764790

Siebert, V., and others. 2023. HIPPO environmental monitoring: Impact of phytoplankton dynamics on water column chemistry and the sclerochronology of the king scallop (*Pecten maximus*) as a biogenic archive for past primary production reconstructions. Earth Syst. Sci. Data **15**: 3263–3281. doi:10.5194/ESSD-2023-39

Spilling, K., and others. 2018. Shifting diatom-dinoflagellate dominance during spring bloom in the Baltic Sea and its potential effects on biogeochemical cycling. Front. Mar. Sci. **5**: 327. doi:10.3389/FMARS.2018.00327

Stecher, H. A., and M. B. Kogut. 1999. Rapid barium removal in the Delaware estuary. Geochim. Cosmochim. Acta **63**: 1003–1012. doi:10.1016/S0016-7037(98)00310-X

Stecher, H. A., D. E. Krantz, C. J. Lord, G. W. Luther, and K. W. Bock. 1996. Profiles of strontium and barium in *Mercenaria mercenaria* and *Spisula solidissima* shells. Geochim. Cosmochim. Acta **60**: 3445–3456. doi:10.1016/0016-7037(96)00179-2

Sternberg, E., D. Tang, T. Y. Ho, C. Jeandel, and F. M. M. Morel. 2005. Barium uptake and adsorption in diatoms. Geochim. Cosmochim. Acta **69**: 2745–2752. doi:10.1016/j.gca.2004.11.026

Strohmeier, T., Ø. Strand, and P. Cranford. 2009. Clearance rates of the great scallop (*Pecten maximus*) and blue mussel (*Mytilus edulis*) at low natural seston concentrations. Mar. Biol. **156**: 1781–1795. doi:10.1007/s00227-009-1212-3

Subba Rao, D. V., Y. Pan, and K. Mukhida. 1998. Production of domoic acid by *Pseudo-nitzschia multiseries* Hasle, affected by lithium. Mar. Ecol. **19**: 31–36. doi:10.1111/j.1439-0485.1998.tb00451.x

Sun, J., and D. Liu. 2003. Geometric models for calculating cell biovolume and surface area for phytoplankton. J. Plankton Res. **25**: 1331–1346. doi:10.1093/PLANKT/FBG096

Tabouret, H., S. Pomerleau, A. Jolivet, C. Pécheyran, R. Riso, J. Thébault, L. Chauvaud, and D. Amouroux. 2012. Specific pathways for the incorporation of dissolved barium and molybdenum into the bivalve shell: An isotopic tracer approach in the juvenile great scallop (*Pecten maximus*). Mar. Environ. Res. **78**: 15–25. doi:10.1016/j.marenvres.2012.03.006

Tachihana, S., and others. 2020. High productivity of eicosapentaenoic acid and fucoxanthin by a marine diatom *Chaetoceros gracilis* in a semi-continuous culture. Front. Bioeng. Biotechnol. **8**: 602721. doi:10.3389/FBIOE.2020.602721

Tardy, Y., G. Krempp, and N. Trauth. 1972. Le lithium dans les minéraux argileux des sédiments et des sols. Geochim. Cosmochim. Acta **36**: 397–412. doi:10.1016/0016-7037(72)90031-2

Thébault, J., and L. Chauvaud. 2013. Li/Ca enrichments in great scallop shells (*Pecten maximus*) and their relationship with phytoplankton blooms. Palaeogeogr. Palaeoclimatol. Palaeoecol. **373**: 108–122. doi:10.1016/j.palaeo.2011.12.014

Thébault, J., L. Chauvaud, S. L'Helguen, J. Clavier, A. Barats, S. Jacquet, C. Pécheyran, and D. Amouroux. 2009*a*. Barium and molybdenum records in bivalve shells: Geochemical proxies for phytoplankton dynamics in coastal environments? Limnol. Oceanogr. **54**: 1002–1014. doi:10.4319/lo.2009.54.3.1002

Thébault, J., B. R. Schöne, N. Hallmann, M. Barth, and E. V. Nunn. 2009*b*. Investigation of Li/Ca variations in aragonitic shells of the ocean quahog *Arctica islandica*, northeast Iceland. Geochem. Geophys. Geosyst. **10**: Q12008. doi:10.1029/2009GC002789

Thébault, J., and others. 2022. Scallop shells as geochemical archives of phytoplankton-related ecological processes in a temperate coastal ecosystem. Limnol. Oceanogr. **67**: 187–202. doi:10.1002/lno.11985

Toullec, J., D. Vincent, L. Frohn, P. Miner, M. Le Goff, J. Devesa, and B. Moriceau. 2019. Copepod grazing influences diatom aggregation and particle dynamics. Front. Mar. Sci. **6**: 751. doi:10.3389/FMARS.2019.00751

Toullec, J., B. Moriceau, D. Vincent, L. Guidi, A. Lafond, and M. Babin. 2021. Processes controlling aggregate formation and distribution during the Arctic phytoplankton spring

bloom in Baffin Bay. Elementa **9**: 00001. doi:10.1525/ELEMENTA.2021.00001

Turner, J. T., and P. A. Tester. 1997. Toxic marine phytoplankton, zooplankton grazers, and pelagic food webs. Limnol. Oceanogr. **42**: 1203–1213. doi:10.4319/lo.1997.42.5_part_2.1203

Vitousek, P. M., J. D. Aber, R. W. Howarth, G. E. Likens, P. A. Matson, D. W. Schindler, W. H. Schlesinger, and D. G. Tilman. 1997. Human alteration of the global nitrogen cycle: Sources and consequences. Ecol. Appl. **7**: 737–750. doi:10.1890/1051-0761(1997)007[0737:HAOTGN]2.0.CO;2

Wang, W.-X., N. S. Fisher, and S. N. Luoma. 1995. Assimilation of trace elements ingested by the mussel *Mytilus edulis*: Effects of algal food abundance. Mar. Ecol. Prog. Ser. **129**: 165–176. doi:10.3354/MEPS129165

Wasmund, N., J. Kownacka, J. Göbel, A. Jaanus, M. Johansen, I. Jurgensone, S. Lehtinen, and M. Powilleit. 2017. The diatom/dinoflagellate index as an indicator of ecosystem changes in the Baltic Sea 1. Principle and handling instruction. Front. Mar. Sci. **4**: 22. doi:10.3389/FMARS.2017.00022

Westberry, T., M. J. Behrenfeld, D. A. Siegel, and E. Boss. 2008. Carbon-based primary productivity modeling with vertically resolved photoacclimation. Glob. Biogeochem. Cycles **22**: GB2024. doi:10.1029/2007GB003078

Widdows, J., M. N. Moore, D. M. Lowe, and P. N. Salkeld. 1979. Some effects of a dinoflagellate bloom (*Gyrodinium aureolum*) on the mussel, *Mytilus edulis*. J. Mar. Biol. Assoc. UK **59**: 522–524. doi:10.1017/S0025315400042843

Winder, M., and U. Sommer. 2012. Phytoplankton response to a changing climate. Hydrobiologia **698**: 5–16. doi:10.1007/s10750-012-1149-2

Worm, B., and others. 2006. Impacts of biodiversity loss on ocean ecosystem services. Science **314**: 787–790. doi:10.1126/science.1132294

Yamamoto, T., S. J. Oh, and Y. Kataoka. 2004. Growth and uptake kinetics for nitrate, ammonium and phosphate by the toxic dinoflagellate *Gymnodinium catenatum* isolated from Hiroshima Bay, Japan. Fish Sci. **70**: 108–115. doi:10.1111/j.1444-2906.2003.00778.x

Zhao, L., B. R. Schöne, and R. Mertz-Kraus. 2017. Controls on strontium and barium incorporation into freshwater bivalve shells (*Corbicula fluminea*). Palaeogeogr. Palaeoclimatol. Palaeoecol. **465**: 386–394. doi:10.1016/J.PALAEO.2015.11.040

Acknowledgments

Special thanks go to Brigitte Stoll and Ulrike Weis (Max Planck Institute for Chemistry, Mainz) for their help to perform the LA-ICP-MS analyses. We further thank the SCUBA divers Erwan Amice, Thierry Le Bec, Isabelle Bihannic, and Emilie Grossteffan for collecting the bivalves. In addition, we kindly acknowledge Beatriz Beker and Gaspard Delebecq for analyzing the phytoplankton samples. We are also grateful to the crew of the research vessel Albert Lucas for their support during the cruises and also thank the Plateau d'analyze chimique des paramètres de base de l'environnement marin (PACHIDERM) as well as the Pôle Spectrométrie Océan (PSO) for the measurements of the various chemical parameters in seawater. This work has been performed within the framework of the French–German collaborative project HIPPO (HIgh-resolution Primary Production multiprOxy archives), co-funded by the German Research Foundation (DFG) grant to BRS (SCHO 793/21) and the French National Research Agency (ANR) grant to J.T. (HIPPO ANR-18-CE92-0036-01), with support of the Région Bretagne (doctoral grant to V.S.). Open Access funding enabled and organized by Projekt DEAL.

Conflict of Interest

None declared

Submitted 11 April 2023
Revised 19 September 2023
Accepted 23 September 2023

Associate editor: Christelle Not